Composites Part B 175 (2019) 107089

Contents lists available at ScienceDirect

Composites Part B

journal homepage: www.elsevier.com/locate/compositesb

Modeling improved fatigue behavior of sugarcane fiber reinforced epoxy composite using novel treatment method

Ajitanshu Vedrtnam [a,b,c,*], Dheeraj Gunwant [b]

[a] Vinoba Bhave Research Institute, Allahabad, UP, 211004, India
[b] Department of Mechanical Engineering, Invertis University, Bareilly, UP, 243001, India
[c] Translational Research Centre, Institute of Advanced Materials, VBRI, Linkoping, 58330, Sweden

ARTICLE INFO

Keywords:
Fatigue strength
composite treatment
sugar cane
natural fiber composite
FEM

ABSTRACT

The use of natural fiber composites in the fatigue prone structures is limited due to the lower strength and durability when compared to the carbon fiber reinforced polymer composites. The present work focuses on improving the bending cyclic fatigue strength (CFS) of the sugarcane fiber reinforced epoxy composite (SFRPC) by a novel treatment method. The treatment has increased up to 40% fatigue life of SFRPC by fiber and interface strengthening. The fatigue life was evaluated using the standard bending cyclic fatigue test. The SFRPCs were prepared using a specially designed compression molding setup by the hand layup method. The sugar cane fibers (SCF) were treated using the waste glass powder and PVA adhesive. The statistical analysis was conducted to observe the effect of the treatment method, the load ration (R) on CFS of treated/untreated SFRPC. A comparison of CFS of SFRPC (treated/untreated) with CFRPC is presented based on the author's previous work. A finite element based model was constituted for predicting the elastic properties of SFRPC (treated/untreated) at different fiber proportions. Additionally, a finite element (FE) model was constituted using the transient analysis in ANSYS (Explicit Dynamics Module) for obtaining the deformation and Von Mises stress at different R for the corresponding life of the treated/untreated SFRPC sample. A theoretical explanation for improved fatigue behavior of SFRPC was presented using scanning electron microscopy (SEM) micrographs and FE results collectively. The stress-strain-life relations for treated/untreated SFRPC were established. It was found that the shear yielding resulted due to the fracture of the outer glass layer of the SCF resulted in the higher CFS of the treated SERPC.

1. . Introduction

The production of the sugar cane is increasing globally and India is the second largest sugar cane producer (348.4 million tonnes) after Brazil (768.7 million tonnes) in the world [1]. The residue waste from the sugar cane juice extraction (bagasse) is incinerated for the power generation [2]. The use of bagasse powder (BP) is reported in the polymeric composites [3]. A significant amount of bagasse is disposed of as waste in open air causing a risk to the environment. The incinerated bagasse produces a large volume of toxic gases contributing to the global warming effect [4]. It was reported in the literature that the wasted lignocellulosic fibers have the potential to replace strong synthetic fibers such as carbon, aramid, glass, and nylon [5]. The low cost (high volume) sugarcane fiber reinforced epoxy composite (SFRPC) could be a promising alternative for carbon fiber reinforced polymer composites (CFRPC) for the fatigue prone structures to an extent if overall cyclic fatigue strength (CFS), stiffness, swelling due to moisture absorption, and durability of SFRPC could be improved. The improvement in CFS of SFRPC was considered as the first objective of the study.

The performance of SFRPC depends on fiber modification, matrix modification, and interface strengthening [6]. The fibers are modified physically, chemically and biologically by employing radiation [7] calendaring [8], steam explosion treatment [9], and corona discharge [10]. The sugar cane fiber (reinforcement material of the present work) consists of cellulose, hemicellulose, and lignin. The chemical treatments target the elimination of weaker constituents such as hemicellulose and lignin from the fiber surface. The alkali treatment [11] cross-linking and grafting [12], and the introduction of coupling agents for the modification of the surface of fibers [13] are commonly employed methods for fiber treatment. The sugar cane fiber modification affects the thermal

* Corresponding author. Vinoba Bhave Research Institute, Allahabad, UP, 211004, India.
E-mail address: ajitanshu.m@invertis.org (A. Vedrtnam).

https://doi.org/10.1016/j.compositesb.2019.107089
Received 27 November 2018; Received in revised form 23 June 2019; Accepted 1 July 2019
Available online 3 July 2019

conductivity SFRPC [14]. The alkali treatment improves the mechanical properties of SFRPC [15]. The acrylic acid treated bagasse composite has superior mechanical properties than NaOH treated bagasse composites [16]. The laminated composite of sugarcane fiber having a higher number of layers has shown superior mechanical properties [17]. In addition to bagasse [18], mechanical properties of the composites made with sugarcane straw [19] and plasticized sugar palm starch [20] have been reported in the literature. The tensile and bending strengths of the SFRPC have shown improvement with the increase in a weight proportion of fibers from 10% to 30%, the further increment of the fiber proportion has resulted in the inferior strength [21].

The epoxy resins (matrix material of the present work) are the low-molecular-weight monomers which are converted into thermoset epoxies when cured with the curing agent. The epoxy has good mechanical strength, stiffness, electrical and chemical resistance, adhesiveness combined with low cure shrinkage and high-processability. Thus, epoxies are suitable for developing reinforced systems, adhesives, coating materials, electrical encapsulating and chemically resistant materials [22]. However, the poor crack resistance of epoxies under static as well as fluctuating conditions results in their brittle failure during service life [23]. The epoxy resins are modified by the addition of additives and fillers, such as reactive oligomeric compounds, low molecular weight polymers, plasticizers, nano-particles, nano-fillers, and carbon nanotubes to overcome their weaknesses for the improved composite performance [22]. Although the strength of composite depends upon base material, filler concentration, moisture, voids and temperature, the interfacial adhesion between filler and matrix primarily governs their CFS [24]. The interfacial bonding is governed by factors such roughness, presence of functional groups on the fiber surface, matrix-filler chemistry [25], voids, cohesion, residual stresses [26,27], the inclusion of nano species [28] and customized treatment methods [24]. In general, bio-composites have a lower mechanical or chemical interlocking between the fiber and matrix. The hydrophobic polymeric matrix and hydrophilic fiber lead to insufficient adhesive bonding [29]. The reinforcing characteristics of the glass as fiber has been studied and documented in the literature [30–32]. These works have indicated the potential of the glass as a reinforcing agent for the thermoset and thermoplastic matrices. A number of customized methods of natural fiber modification are reported in the literature [33–35] but the effect of surface modifying characteristics of the powdered glass (waste and harmful otherwise) for natural fiber composites is rarely investigated in the cited literature [24]. An inexpensive method with the inexpensive materials for improved performance and the high volume fiber treatment for the production of SFRPC is reported in the present work.

The second objective of the study was to establish the stress-strain-life relationships for the treated and untreated SFRPC. A finite element (FE) model was constituted to determine the stress and strain experienced by the SFRPC samples at different failure loads and associated lives. The life of SFRPC samples was determined by the standard bending cyclic fatigue test [36–38]. The FE modeling of natural fiber composites is reported extensively in the literature [39–43] for determining micromechanical properties (strength, failure, deformation, and damage) [44–48], macro shape deformation (fracture and stress-strain) [49–52] and thermal conductivity [53]. The mesoscale elastic FE model for predicting tensile behavior of single hemp fiber with the different geometrical profile is reported in Ref. [54]. The microscale elastic-plastic model for predicting the tensile behavior of hemp fibers considering the fiber dimension and microstructure is reported in Ref. [55]. A review containing a summary of 113 articles covering the FE modelling of natural fibers for different length scales, thermal and mechanical properties is reported by Ref. [56]. The representative volume element model and multi-scale homogenization-based constitutive method have effectively investigated the effect of microstructures on the mechanical properties of natural fibers composites. Thus, these approaches were adopted in the present work. The bulk elastic properties of treated and untreated SFRPCs were predicted through a micromechanical FE model coupled with the numerical homogenization technique.

The final objective of the study was to establish the structure-property relationship and providing a theoretical explanation on the mechanism the fracture of SFRPC. As the fatigue loading is most frequently responsible for the failure of engineering structures [57,58], determining and improving along with modeling fatigue life of a potentially important engineering composite SFRPC becomes imperative. The fatigue failure of the composites occurs due to the propagation of matrix cracks, delamination, longitudinal splitting, and fiber fracture [59]. However, matrix cracking is the first form of fracture and does not result in catastrophic failure. The fatigue failure depends on the microstructure the fiber architecture [57–59]. The longitudinal splitting is governed by intra-laminar shear fracture which encourages delamination [60]. The SEM micrographs of fractured SFRPC samples and FE modeling results were utilized for achieving the final objective.

The method used for improving the CFS of SFRPC is inspired by the author's previous work [24] but novel in nature. The FE modeling approach used in the study is widely accepted but not cited in the literature for modeling behavior of treated and untreated SFRPC under bending cyclic fatigue loading. The developed FE model would be useful for predicting CFS of other powder reinforced composites. Further, the FE model compliments SEM micrograph for determining the strengthening mechanisms of SFRPC due to the treatment. The statistical analysis was conducted for ensuring the validity of the experimental results for the population and interpreting the data from experimentation and simulation. The methodology for untreated and treated SFRPC preparation, fatigue testing, FE modeling, and statistical analysis has been explained in the materials method section. The results and discussion section encompasses experimental, statistical, morphological, and numerical results. Finally, the conclusive outcomes and future extensions of the present study were discussed.

2. . Materials and methods

2.1. Fiber treatment and composite preparation

The bagasse particles (BP), Bisphenol A diglycidyl ether (DGEBA) based epoxy resin (LY 556), curing agent triethylenetetramine (HY 951), poly vinyl acetate (PVA) based adhesive and the waste glass powder were utilized for the fabrication of the SFRPC samples. The sugar cane fiber consists of 40–45% cellulose, 20–28% hemicellulose, and 20–25% lignin. The BPs were ground to the particle size ranging 100–600 μm prior to the composites preparation using sieve analysis. The specially designed mould was fabricated for the preparation of composites so that minimum post curing processing is required.

The composites were prepared by the traditional hand-lay-up technique [24]. The epoxy resin and curing agent were mixed thoroughly in the ratio 1:1 at the room temperature with subsequent addition of 20, 25 and 35 vol % BPs (untreated/treated). The total weight of one sample (20% volume proportion of BP) used for fatigue testing was 19 g, 8 gm each of epoxy and hardener and remaining was of BP. The mixture of epoxy resin, curing agent and BP was then poured in the mould smeared with silicon grease to allow easy withdrawal. The mould was subjected to a dead load of 10 kg in order to obtain a strong, dense, and non-porous casting [24]. The casting was post-cured for 24 h in the air after removal from the mould. The treated BPs were first coated PVA based adhesive followed by the glass powder coating around them. Further, the treated particles were left for drying for 24 h at the room temperature. The dried particles were visually inspected for any non-uniformity in the treatment and further, the sieve analysis was performed for having uniformity in the size of treated BPs. The composite samples consisting of treated particles were prepared using the method identical to that employed for untreated ones. Fig. 1. (a)-(e) show photographs of untreated and treated bagasse particles, sieve analysis apparatus, specially designed mould and samples curing in the mould under steady load and SFRPC

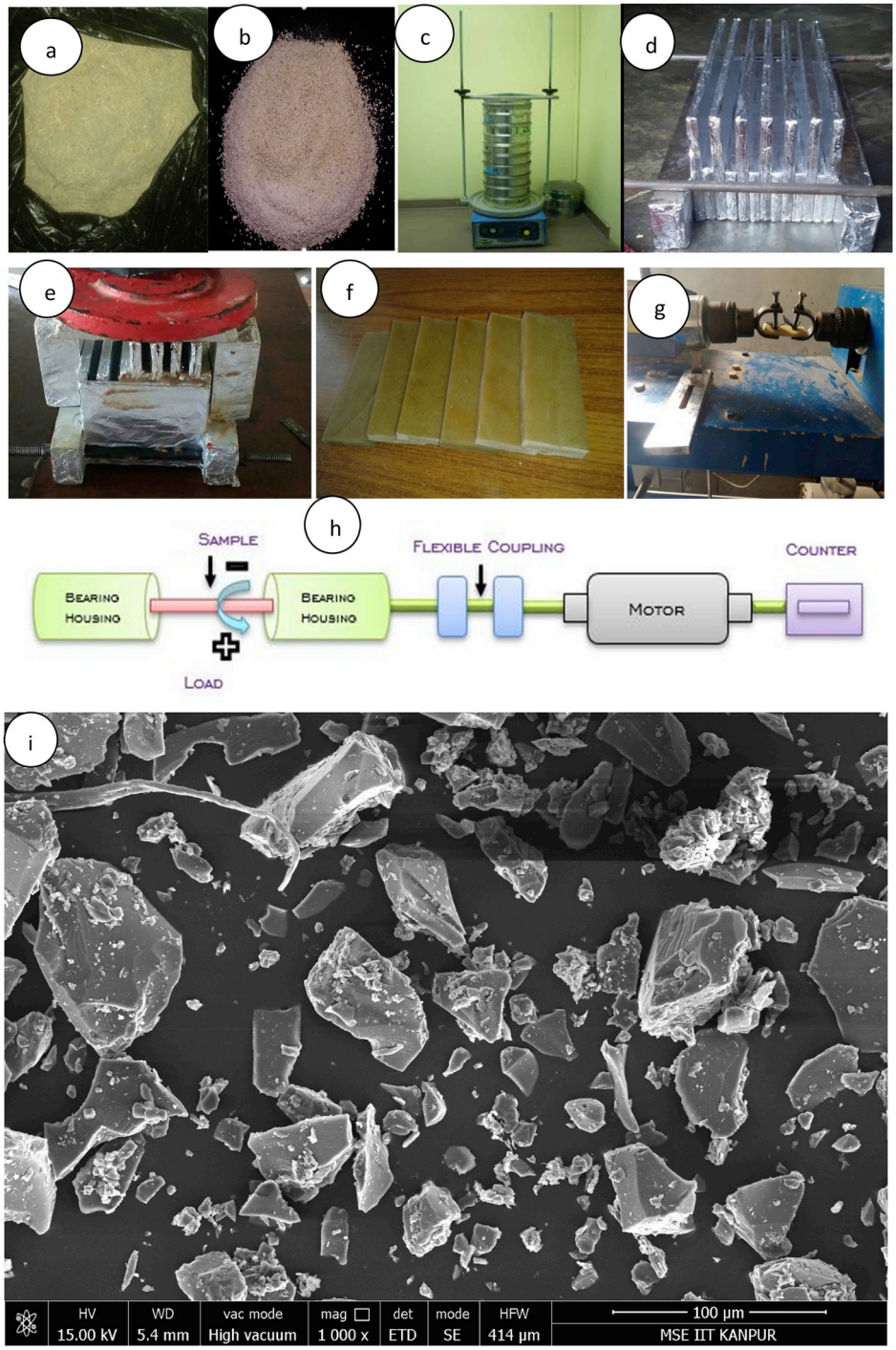

Fig. 1. (a) Untreated bagasse particles (b) Treated bagasse particles (c) Sieve analysis apparatus (d) Specially designed mould (e) Sample curing in mould under steady load (f) SFRPC samples (g) Fatigue testing machine with fixture holding SFRPC sample before fatigue testing (h) Block diagram of fatigue testing setup (i) SEM micrograph of BPs.

samples respectively. Fig. 1 (i) shows the SEM micrograph of BPs.

2.2. Fatigue testing

The cast iron fixtures with rubber pads were used for providing damage-free tight grip while holding the samples during fatigue test. The specimen size for fatigue test was taken to be $8 \times 6\ cm^2$. Fig. 1 (g) and (h) shows the fatigue testing machine fixture used and the block diagram of the experimental set-up. An alternating bending load varying between minimum and maximum values was applied to the specimens. The minimum load was kept fixed at 1 kg (9.81 N) and the maximum load was varied in the range between 4 kg (39.24 N) to 16 kg (156.96 N) with an increment of 3 kg (29.43 N). The maximum load ratio (R) (ratio of minimum load to the maximum load) was taken as 0.25. The fatigue testing machine automatically stops once the sample is fractured. The numbers of cycles at which SFRPC samples were fractured were recorded.

2.3. Finite element modeling

The elastic properties of bulk material were predicted using the numerical homogenization technique. In the model, the treated/untreated

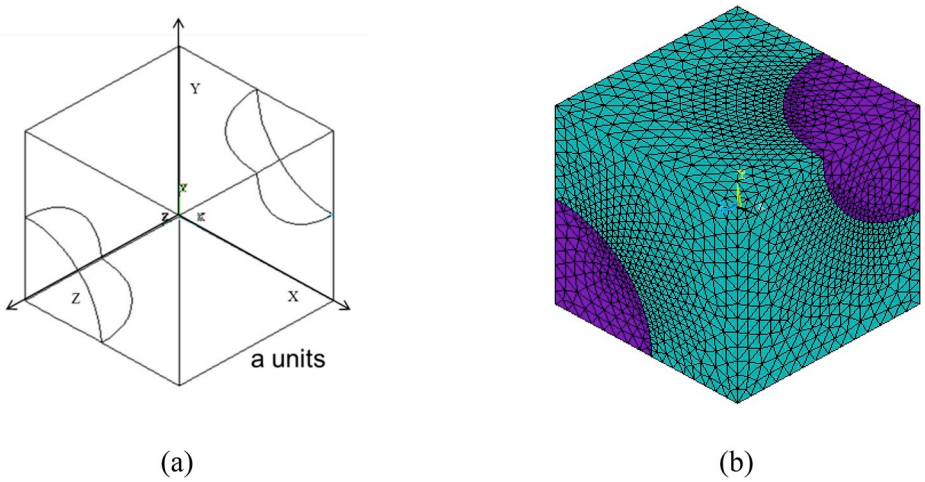

Fig. 2. BCC unit cell and FE model (a) without meshing and (b) with meshing.

Table 1
Material properties of various constituent used in the FE analysis [24,63–65].

S. No.	Constituent	Young's modulus (MPa)	Poisson's ratio
1	Epoxy	3500	0.33
2	BP	11000	0.33
3	Glass	70000	0.23

BPs were assumed to be distributed evenly in the epoxy matrix in body-centered cubic (BCC) pattern as shown in Fig. 2. The FE model was assumed to be a representative volume of size a x a x a μm^3 located at the top portion of the fatigue testing specimen (above the neutral axis). At any particular instant, the top-most fibres of a bending specimen are subjected to a tensile stress and the bottom-most fibres are subjected to compressive stress.

The BCC model is a multi-inclusion model which assumes the BCC distribution of BPs in the epoxy matrix. It is a periodic model that

Table 2
Experimentation and simulation results.

S. No.	Proportion (%)	R	Load variation	No. of cycles (untreated)	Von-Mises stress (MPa) (untreated)	Deflection (mm) (untreated)	No. of cycles (treated)	Von-Mises stress (MPa) (treated)	Deflection (mm) (treated)
1	**20**	**0.25**	**−9.81 to +39.24**	**1970**	**17.414**	**0.0526**	**2520**	**17.425**	**0.0496**
2	**20**	**0.25**	**−9.81 to +39.24**	**1874**	**17.398**	**0.0505**	**2475**	**17.414**	**0.0434**
3	25	0.25	−9.81 to +39.24	2022	17.354	0.0472	2722	17.428	0.0466
4	25	0.25	−9.81 to +39.24	2124	17.418	0.0499	2645	17.245	.0425
5	**35**	**0.25**	**−9.81 to +39.24**	**1875**	**17.405**	**0.0428**	**2345**	**17.434**	**0.0411**
6	**35**	**0.25**	**−9.81 to +39.24**	**1954**	**17.421**	**0.0451**	**2274**	**17.425**	**0.0399**
7	20	0.14	−9.81 to +68.67	980	30.361	0.104	1260	30.38	0.0978
8	20	0.14	−9.81 to +68.67	924	30.351	0.0981	1158	30.32	0.0945
9	**25**	**0.14**	**−9.81 to +68.67**	**1014**	**30.359**	**0.0897**	**1524**	**30.376**	**0.0824**
10	**25**	**0.14**	**−9.81 to +68.67**	**1154**	**30.366**	**0.0987**	**1653**	**30.386**	**0.0919**
11	35	0.14	−9.81 to +68.67	892	30.372	0.089	1140	30.384	0.074
12	35	0.14	−9.81 to +68.67	884	30.370	0.074	1248	30.395	0.081
13	**20**	**0.1**	**−9.81 to +98.1**	**770**	**43.305**	**0.132**	**960**	**43.331**	**0.138**
14	**20**	**0.1**	**−9.81 to +98.1**	**845**	**43.311**	**0.155**	**989**	**43.338**	**0.146**
15	25	0.1	−9.81 to +98.1	994	43.338	0.147	1154	43.341	0.125
16	25	0.1	−9.81 to +98.1	1091	43.328	0.128	1204	43.346	0.137
17	**35**	**0.1**	**−9.81 to +98.1**	**675**	**43.327**	**0.132**	**896**	**43.360**	**0.121**
18	**35**	**0.1**	**−9.81 to +98.1**	**588**	**43.320**	**0.121**	**888**	**43.348**	**0.113**
19	20	0.07	−9.81 to +127.53	510	56.261	0.206	880	56.290	0.181
20	20	0.07	−9.81 to +127.53	485	56.254	0.186	908	56.298	0.194
21	**25**	**0.07**	**−9.81 to +127.53**	**651**	**56.268**	**0.181**	**991**	**56.308**	**0.182**
22	**25**	**0.07**	**−9.81 to +127.53**	**689**	**56.272**	**0.196**	**984**	**56.301**	**0.162**
23	35	0.07	−9.81 to +127.53	460	56.282	0.176	789	56.327	0.161
24	35	0.07	−9.81 to +127.53	425	56.275	0.160	771	56.322	0.142
25	**20**	**0.06**	**−9.81 to +156.96**	**440**	**69.213**	**0.257**	**620**	**69.251**	**0.205**
26	**20**	**0.06**	**−9.81 to +156.96**	**384**	**69.210**	**0.224**	**648**	**69.258**	**0.242**
27	25	0.06	−9.81 to +156.96	510	69.220	0.202	745	69.24	0.198
28	25	0.06	−9.81 to +156.96	526	69.226	0.245	776	69.27	0.228
29	**35**	**0.06**	**−9.81 to +156.96**	**430**	**69.239**	**0.220**	**589**	**69.293**	**0.201**
30	**35**	**0.06**	**−9.81 to +156.96**	**384**	**69.235**	**0.184**	**501**	**69.284**	**0.171**

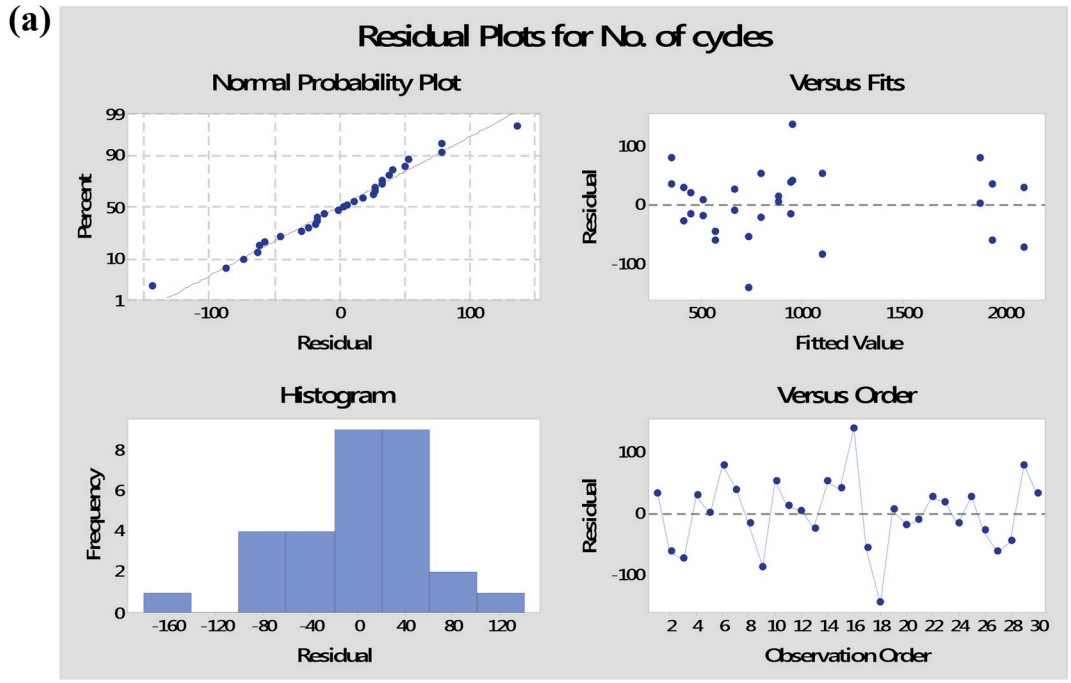

Fig. 3a. Residue plots for no. of cycles withstand by the untreated SFRPC samples.(see.Fig. 3b)

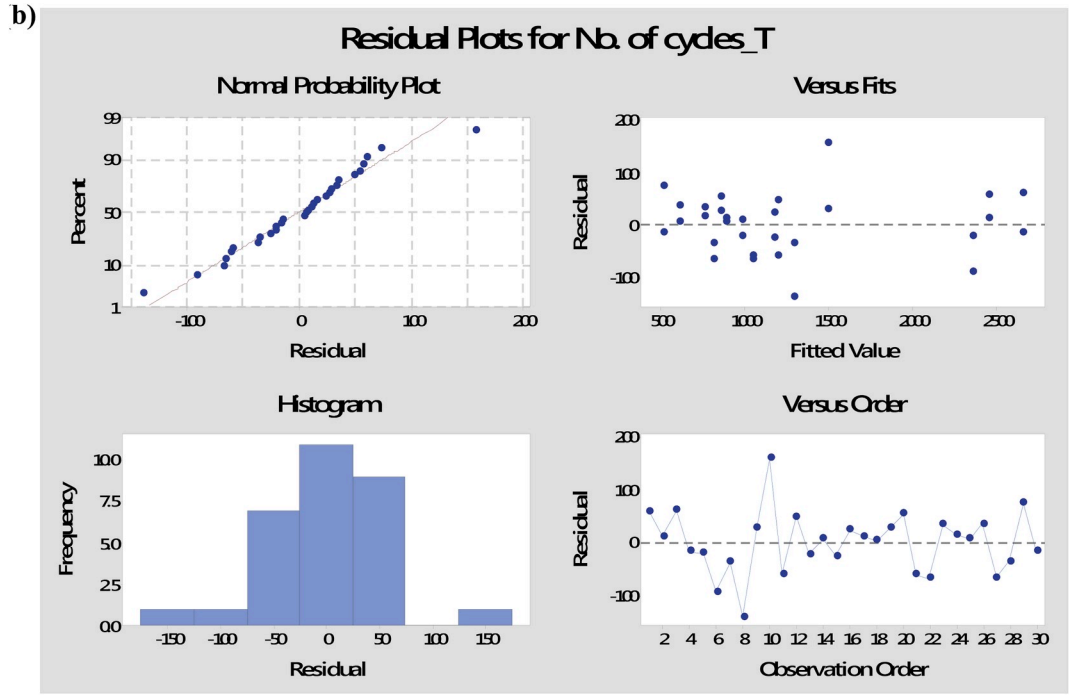

Fig. 3b. Residue plots for no. of cycles withstand by the treated SFRPC samples.

considers the effect of adjacent BPs on the stress distribution. The FE procedure was made computationally efficient by modeling a one-eighth model of the BCC unit cell. A total of 24,200 3D solid95 tetrahedral elements available in the library of ANSYS were employed to discretize the model. The mesh was refined until mesh independence was observed in the results. The similar modeling approach and boundary conditions were employed by the authors for predicting the elastic properties and stress distributions in liquid rubber modified epoxy [61].

The symmetric boundary conditions were applied on the X = 0, Y = 0 and Z = a μm planes considering Y-Z as the plane of bending. A uniform displacement was applied on the Z = 0 plane in the model. After the solution was completed, average stresses and strains were calculated. The Young's modulus was calculated by dividing the average stress in Z direction with corresponding average strain. The Poisson's ratio was calculated by dividing strain in Y direction with the strain in Z direction [62]. The numerical homogenization technique and post-processing commands were implemented through an ANSYS parametric design language (APDL) macro. The model was further employed to understand the behaviour of the untreated as well as treated bagasse particle reinforced composites on the stress concentrations in the composites. The

(a)

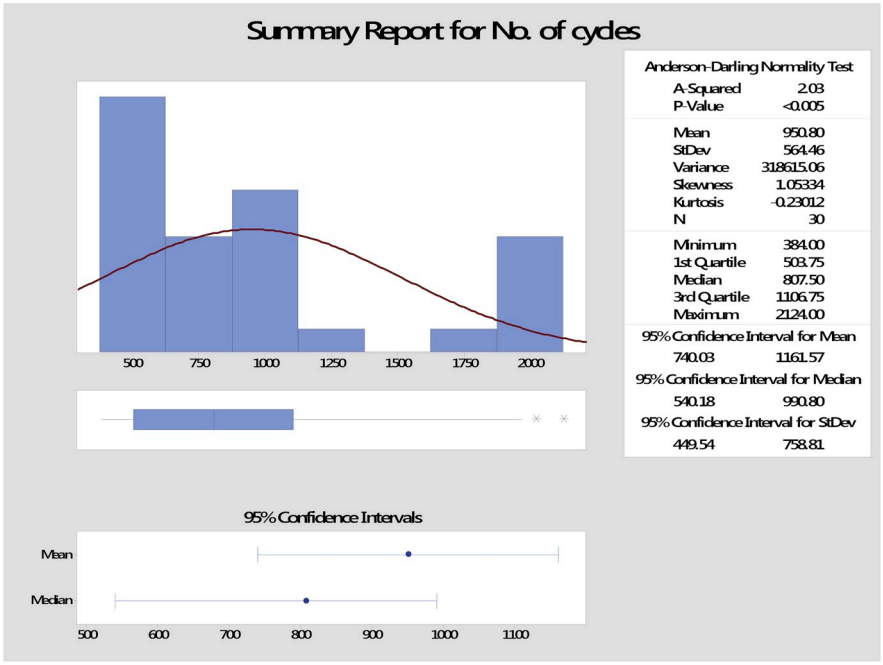

Fig. 4a. The statistical summary the untreated SERPC samples.

(b)

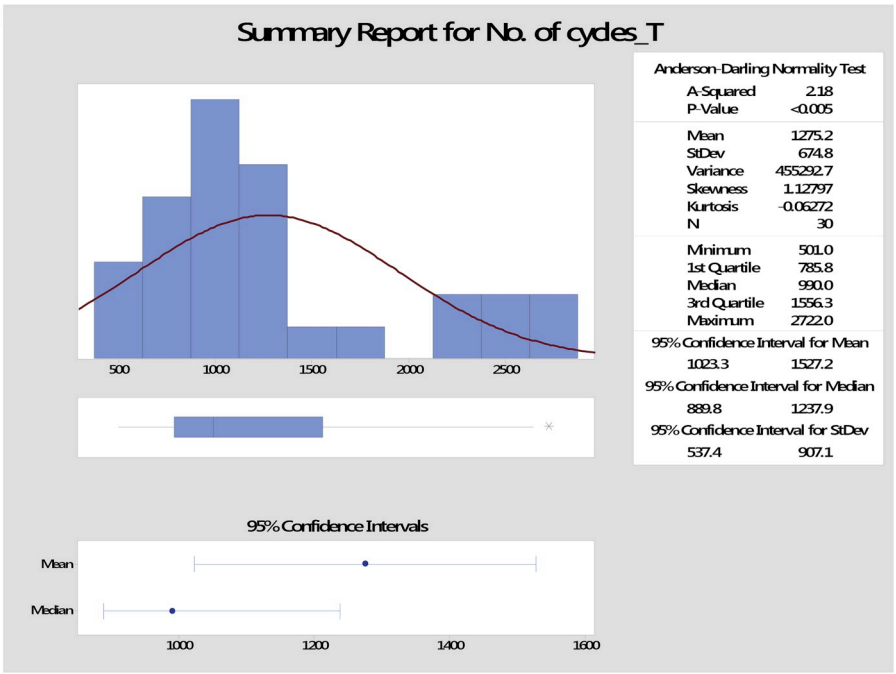

Fig. 4b. The statistical summary the treated SFRPC samples.

boundary conditions were applied to simulate the effect of experimental bending of the specimen during fatigue testing. A linear elastic material model was chosen to model the behaviour of constituents and the analysis was conducted. Table 1 displays the material properties of various constituents used in the analysis [24,63–65].

Further, a macro-mechanical FE model was constituted to obtain theVon Mises stresses and deflection for associated values of R and number of cycles. The fatigue test was simulated using the Explicit Dynamics Module of (transient analysis) ANSYS. Table 1 gives the properties of BPs [65], glass [63,64], and epoxy [24] (assuming the glass as continuous) used for modeling. The loading and boundary conditions were taken from the experimentation. The SFRPC sample was kept fixed at the corners using nodal restraints and only rotation was allowed while the cyclic bending load was applied. The linear elastic material model is considered for the study [66,67]. The mesh statics includes 38234 solid 95 mesh elements with an average element quality of 0.5679. The grid refinement was performed to examine any noteworthy change. The maximum deformation (MD) and maximum Von Mises stress were calculated considering RPM 1200 (as was in experiments), the associated value of R and the maximum number of cycles withstand by the samples before the fracture during experiments. The time duration for which the cyclic bending load was applied during simulation was calculated by dividing a total number of cycles withstand by the samples by 1200 (RPM of fatigue testing machine). The statistical analysis was

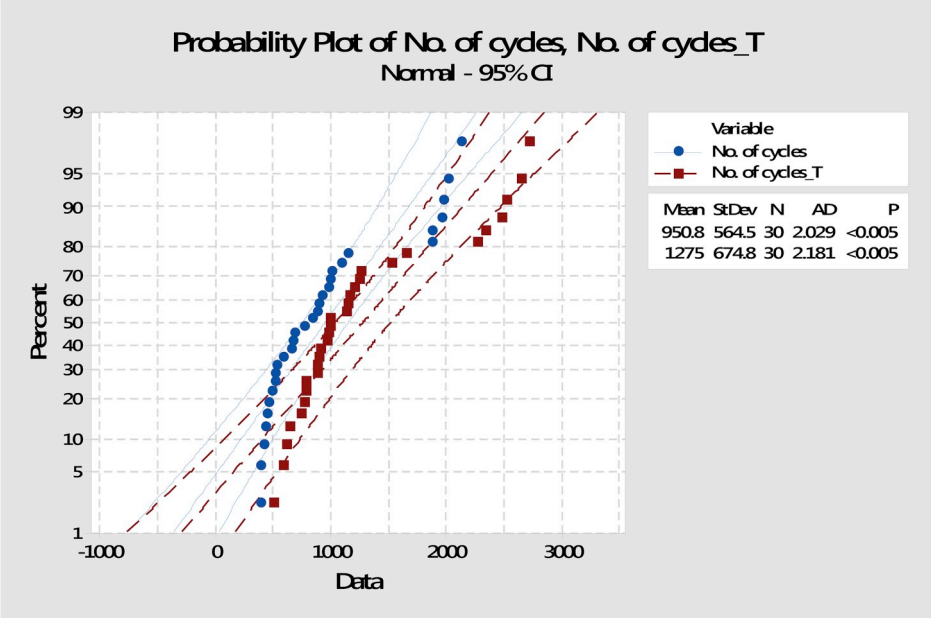

Fig. 5. The probability plots for no. of cycles of the untreated and treated SERPC samples.

performed using MINITAB.

3. . Results and discussion

3.1. Fatigue testing

Table 2 gives the results of the bending cyclic fatigue testing of 30 untreated and 30 treated SFRPC samples. The SFRPC samples (treated/untreated) were having the longest life at 25% proportion of BPs. At the 20% proportion and R = 0.25, the untreated samples sustained 1970 cycles whereas the treated samples have sustained 2520 cycles (28% higher than the untreated ones). This indicates the inclusion of the glass powder at the outer layer of BPs possibly enhanced the stress transfer between the BPs due to interface strengthening. The similar reinforcing behaviour of silica on the epoxy matrix was reported by Constantinescu et al. [68]. The significant enhancement in the fatigue crack growth resistance of the silica particle reinforced matrix in comparison with unmodified epoxy was possibly due to crack deflection and pinning phenomenon at rigid particles [69].

The life of the treated/untreated SFRPC samples decreases as the R reduces (load increases). The number of cycles sustained by untreated SFRPC (20% BPs) for R = 0.25 and R = 0.06 were 1970 and 440 cycles (347% lesser) respectively. This result is obvious due to the fact that as the severity of load increases, the no. of cycles before failure reduce drastically [36,48,49]. The similar trends were observed for treated SFRPC; however, the untreated SFRPC samples were having 28.79% (for R = 0.25) and 40.90% (for R = 0.06) the lesser life than the treated SFRPC samples. The number of cycles sustained by untreated SFRPC (25% BPs) for R = 0.25 and R = 0.06 were 2124 and 526 cycles (303.8% lesser) respectively. The untreated SFRPC samples were having 30.58%

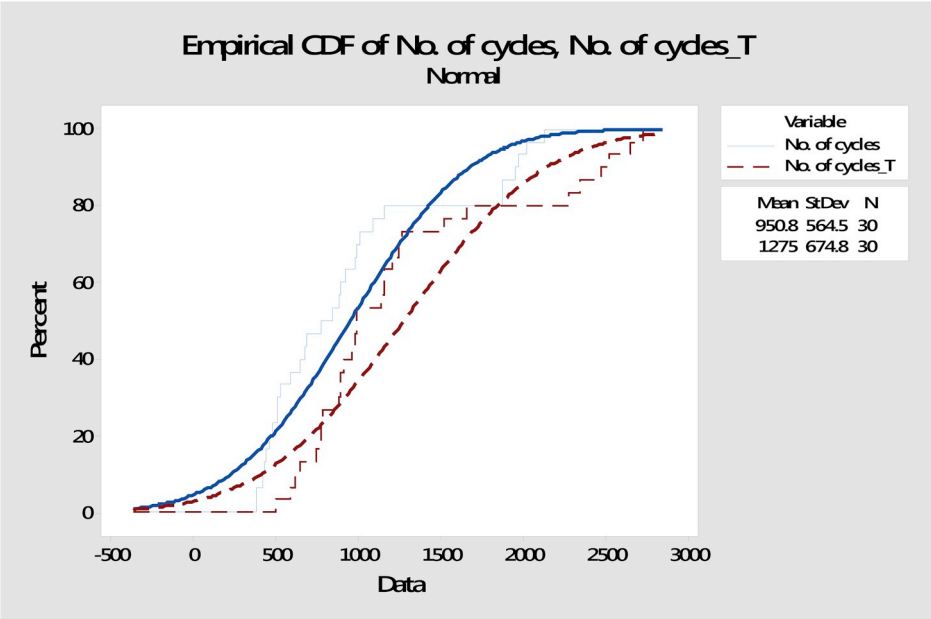

Fig. 6. The empirical CDF plots for the untreated and treated SERPC samples.

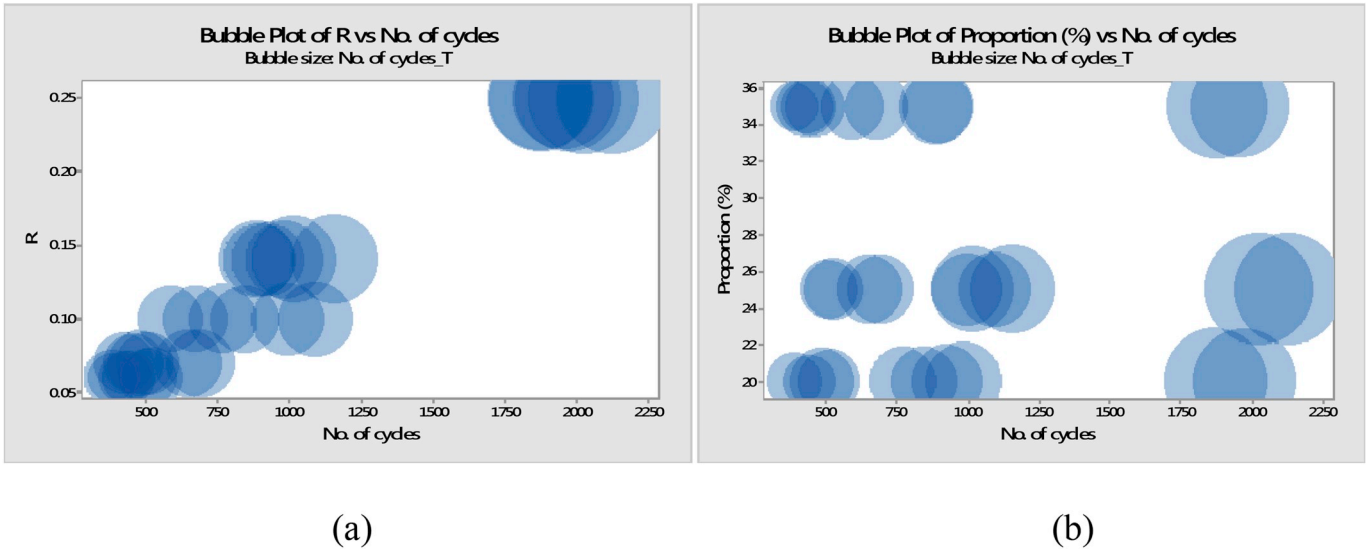

Fig. 7. Bubble plots (a) R vs No. of cycles (b) Proportion (%) vs No. of cycles for untreated SFRPC samples.

(for R = 0.25) and 36.97% (for R = 0.06) the lesser life than the treated SFRPC samples. The similar trends are observed for 35% volume proportion of reinforced fibers; however, the treated/untreated SFRPCs were having the highest life for 25% volume fraction of fibers, followed by 35% and 20% volume fraction respectively. The treated samples SFRPC samples have sustained significantly higher no. of cycles prior to fracture in comparison with the untreated particles irrespective for all associated R and proportions of fibers. This might be due to the effective mechanical interaction at glass-powder/epoxy interface in treated particle composites. The glass particles have been observed to induce crack pinning and shear yielding of epoxy matrix improving its mechanical properties [70]. The localized shear yielding could be the main reason behind enhanced fatigue resistance of composites with treated particles. The life of SFRPC was decreased above 25% fiber proportion (for the tested proportions). This could be due to agglomeration of BPs leading to the heterogeneous distribution of reinforcement and formation of stress concentration sites. The agglomeration of particles promotes the initiation and growth of fatigue crack [71]. The reduced inter particle distance at higher concentrations is also attributable to retarded shear yielding of the epoxy matrix [72].

The Von-Mises stress (MPa) for untreated SFRPC (20% fibers) varied from 17.414 (for R = 0.25) to 69.213 (297% higher) for R = 0.06. This shows that reduction in R resulted in higher Von-Mises stress. The deflection (mm) increased about 388% from 0.0526 (for R = 0.25) to 0.257 (for R = 0.06) and 20% fiber proportion. On the other hand, the treated SFRPC samples showed nearby Von-Mises stress values to untreated SFRPC, but significantly lower deflection. For R = 0.25 and 20% proportion, the deflection in treated SFRPC sample was 5.70% lesser than untreated SFRPC samples. As the proportion of fibers was increased from 20 to 35% R = 0.1, the deflection was reduced from 0.155 to 0.132 (14.84% less). In the case of treated SFRPC sample, the deflection reduced from 0.146 to 0.121(17.12% lesser). It can be observed that at same R, increasing the proportion had a more significant effect in the case of treated SFRPC sample. At all proportions and loading ratios, the treated samples were observed to have lesser deflection than the untreated samples. This indicates the strengthening effect due to the treatment of SFRPCs. The reduction in deflection is attributed to the presence of high modulus glass-powder layer. The similar trend was observed for the higher proportion of fiber as well. Further, for an insight and examining the validity of the experimental results, Analysis of variance (ANOVA), Regression Analysis and other statistical analyses were conducted for untreated and treated SFRPCs. The ANOVA for the

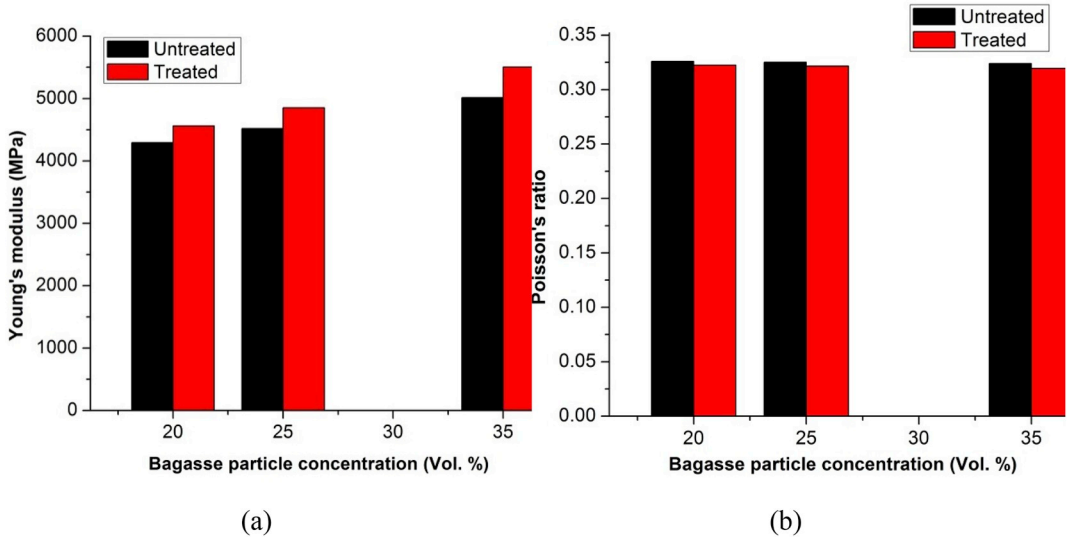

Fig. 8. Variation of predicted (a) Young's modulus and (b) Poisson's ratio for untreated and treated bagasse particle reinforced composites.

no. of cycles for the untreated SFRPCs samples are as follows.

Factor Information.

Factor	Type	Levels	Values
R	Fixed	5	0.06, 0.07, 0.10, 0.14, 0.25
Proportion (%)	Fixed	3	20, 25, 35

Analysis of Variance.

Source	DF	Adj SS	AdjMS	F-Value	P-Value
R	4	8885699	2221425	541.05	0.000
Proportion (%)	2	259705	129852	31.63	0.000
Error	23	94433	4106		
Lack-of-Fit	8	54400	6800	2.55	0.056
Pure Error	15	40033	2669		
Total	29	9239837			

Model Summary.

S	R-sq	R-sq(adj)	R-sq(pred)
64.0764	98.98%	98.71%	98.26%

The ANOVA results clearly reflect that R and proportion (%) significantly affect the life of untreated SFRPC. R is more significant than proportion (%) as reflected by the higher F-value. These observations are valid for the population as the p-value is lesser than 0.05. Equation (1) gives the regression equation for the untreated SFRPC useful for predicting the fatigue life of the untreated SFRPCs in between the tested values.

No. of cycles = 950.8–505.1 R_0.06–414.1 R_0.07–123.6R_0.10 + 23.9 R_0.14 + 1019.0R_0.25–32.6Proportion (%)_20 + 126.7 Proportion (%) _25–94.1 Proportion (%)_35. (1)

The residue plots (Fig. 3 (a) and Fig. 3 (b)) clearly reflect that the data qualifies the thick pencil test, the error is within consideration limits and the data is normally distributed. For the treated SFRPC, following are the results of ANOVA.

Analysis of Variance.

Source	DF	Adj SS	AdjMS	F-Value	P-Value
R	4	12653382	3163345	756.72	0.000
Proportion (%)	2	453959	226980	54.30	0.000
Error	23	96148	4180		
Lack-of-Fit	8	63271	7909	3.61	0.016
Pure Error	15	32878	2192		
Total	29	13203489			

Model Summary.

S	R-sq	R-sq(adj)	R-sq(pred)
64.6557	99.27%	99.08%	98.76%

The similar conclusions can be deduced from the ANOVA results of treated SFRPCs as were for untreated SFRPCs and equation (2) gives the regression equation for the untreated SFRPC samples.

No. of cycles_T = 1275.2–628.7R_0.06–388.1R_0.07–260.1 R_0.10 + 55.3R_0.14 + 1221.6R_0.25–33.4 Proportion (%)_20 + 164.6 Proportion (%) _25–131.1 Proportion(%)_35 …. (2)

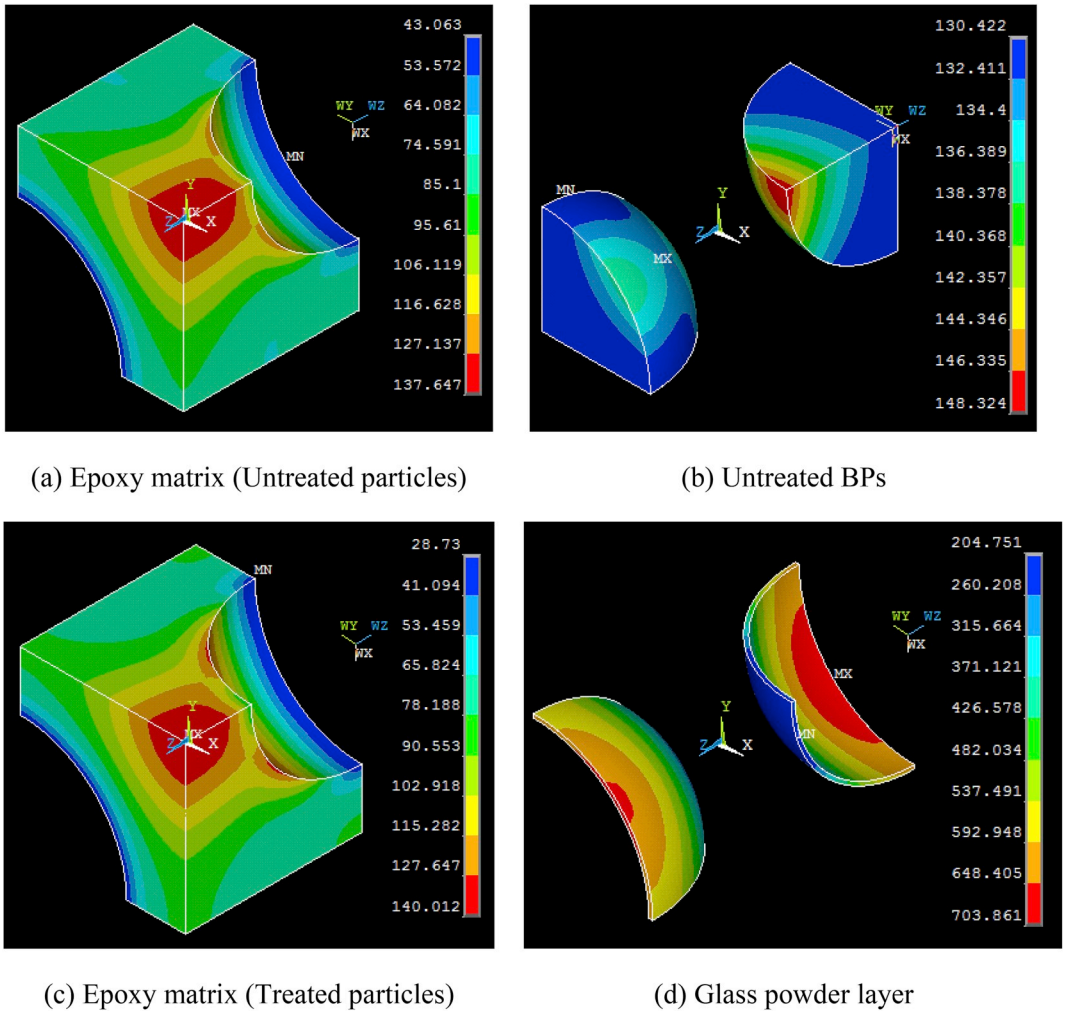

(a) Epoxy matrix (Untreated particles)

(b) Untreated BPs

(c) Epoxy matrix (Treated particles)

(d) Glass powder layer

Fig. 9. (a–i). Variation of stresses in epoxy, bagasse particle and the glass layer for different cases.

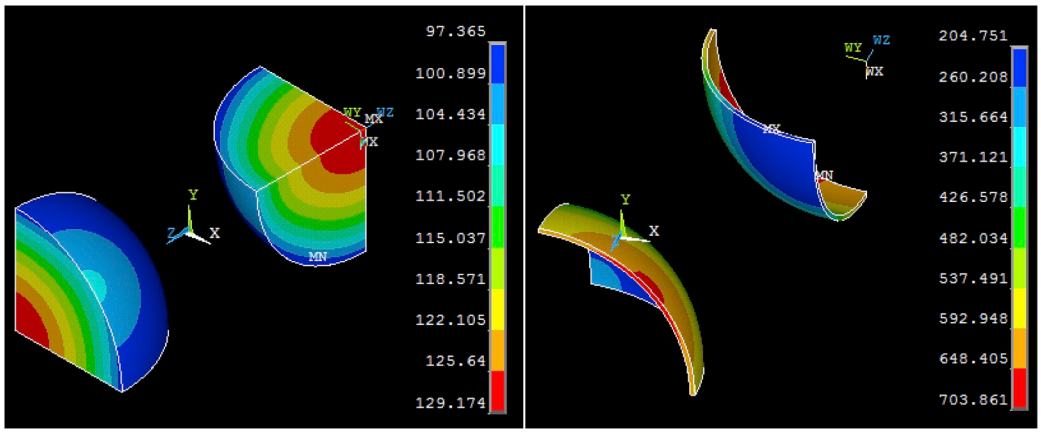

(e) Treated BPs (f) Glass powder layer

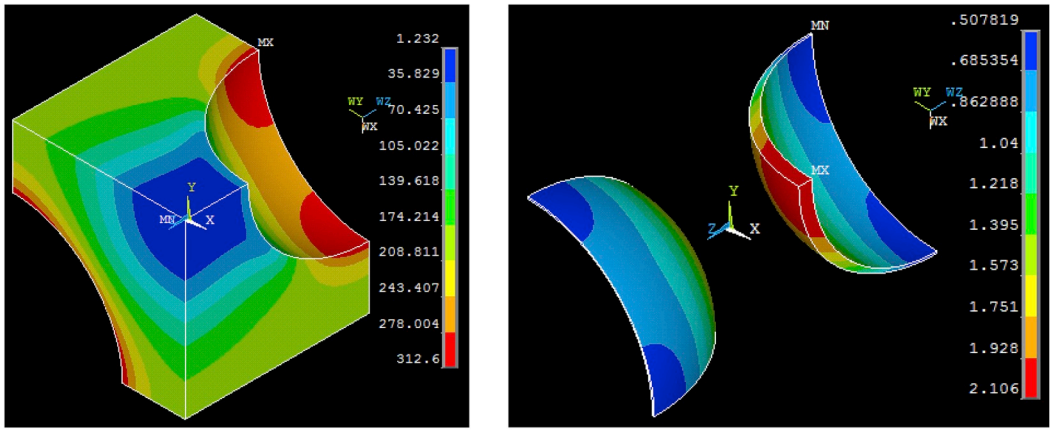

(g) Stress distribution in epoxy post-fracture of glass layer (h) Stress distribution in glass layerpost-fracture

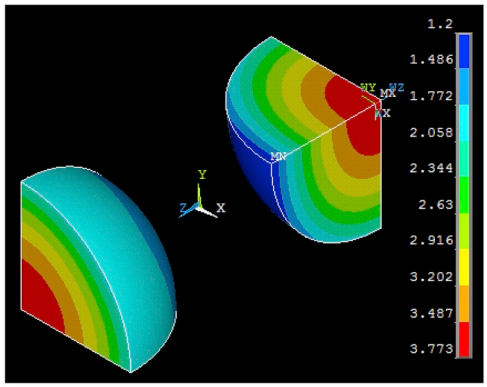

(i) Stress distribution in BPs post-fracture of the glass layer.

Fig. 9. (*continued*).

Fig. 4 (a) and Fig. 4 (b) shows the statistical report for no. of cycles including Anderson-Darling normality test, mean, standard deviation, variance, skewness, kurtosis and box plots for untreated and treated SFRPCs respectively. The Anderson-Darling normality test results indicate that the data is normally distributed for both treated and untreated SFRPCs, the constituted probability plots (Fig. 5) have confirmed data represents the population keeping error within the limits. The skewness of data for the treated samples is approaching to zero more closely thus the data for treated sample is having higher symmetry.

Fig. 5 shows the probability plot for the number of cycles in treated and untreated SFRPCs. The probability plot shows that the treated/untreated SFRPCs follow the normal distribution. The data points in both the cases were observed to follow the straight line and thus, can be considered as a good fit. The mean values of the number of cycles for

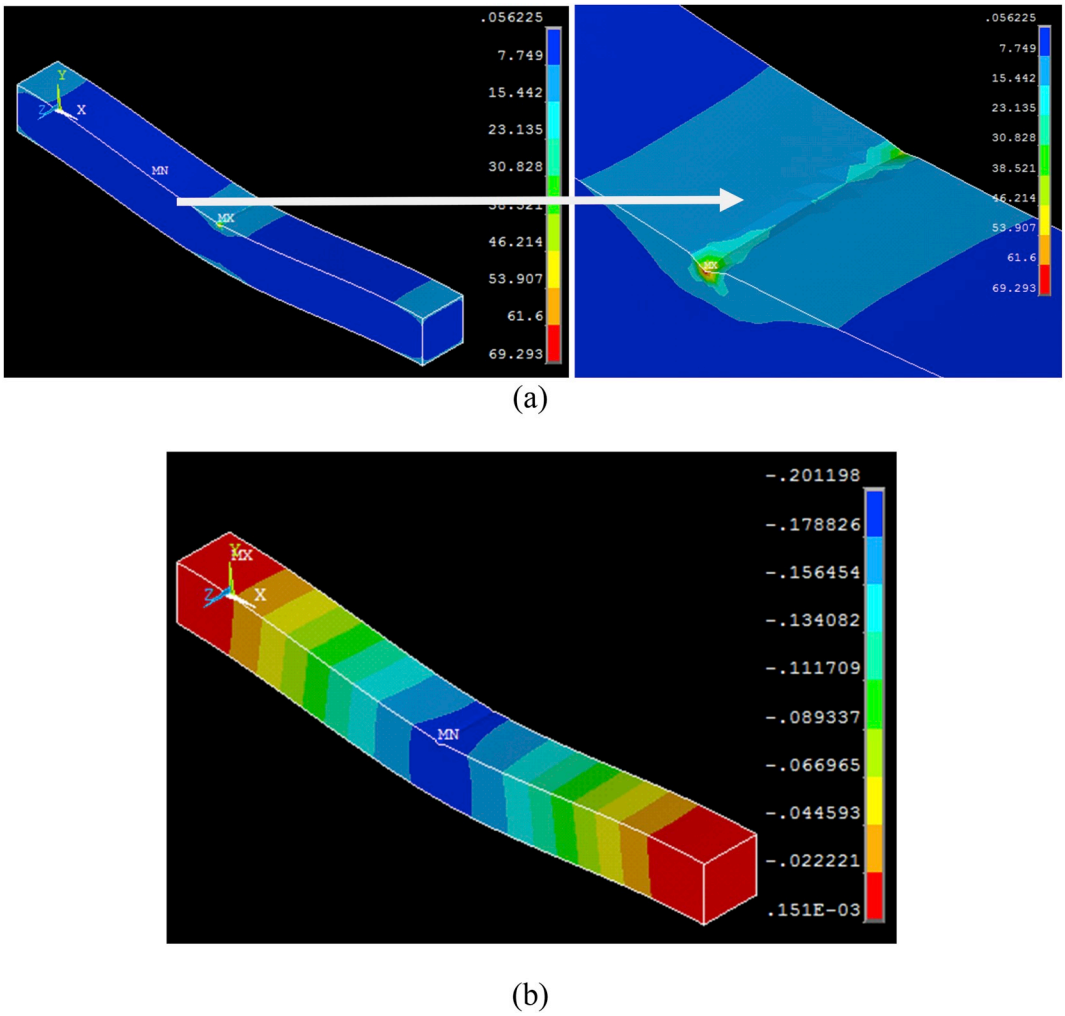

Fig. 10. Sample modeling results (a)Von-Mises stress (MPa) (b)Deflection (mm) (Untreated) for R = 0.07, Proportion (%) = 20%, N = 500.

untreated and treated SFRPCs were observed to be 950.8 and 1275 respectively. On an average, the treated SFRPCs sustained 34.09% higher number of cycles than the untreated SFRPCs.

The fit of distribution of data in empirical CDF (Fig. 6) confirms the superiority of treated SFRPC samples over untreated SFRPC for the population. The empirical CDF clearly indicate improvement in the fatigue life of SFRPC for the population after the treatments.

As it is clear that the untreated and treated SFRPC samples follows

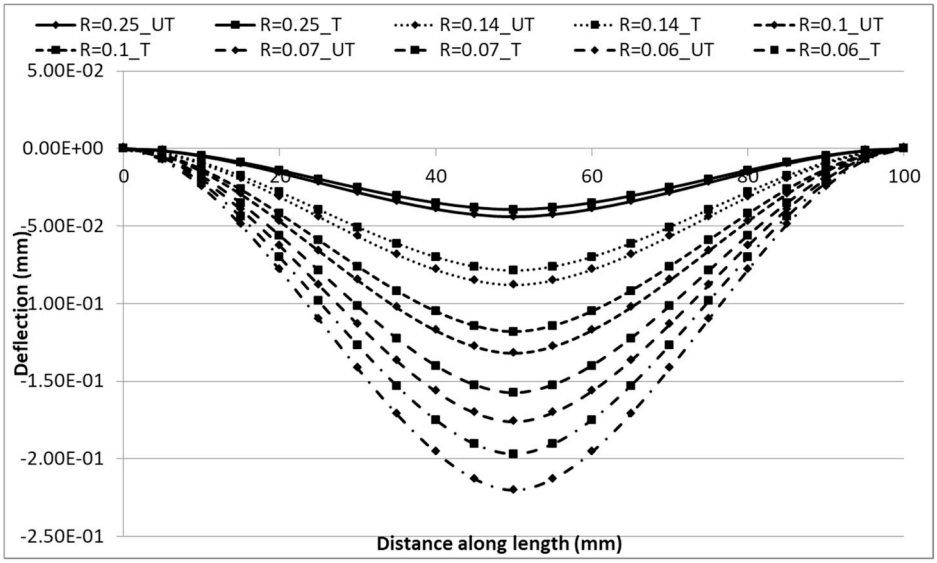

Fig. 11. Mid-line deflection (vol. % = 20) of Untreated (UT) and Treated (T) SFRPC samples.

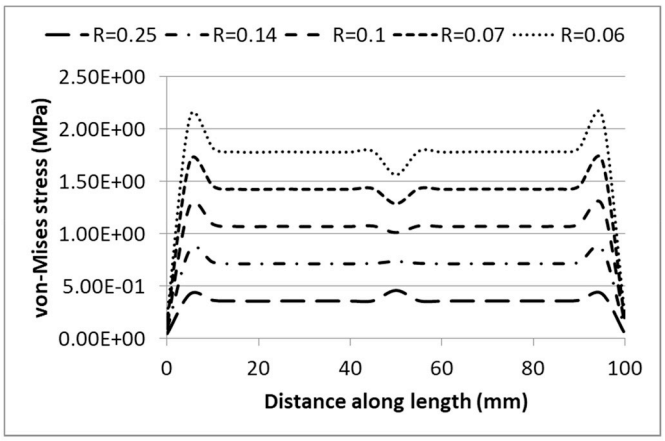

(a)

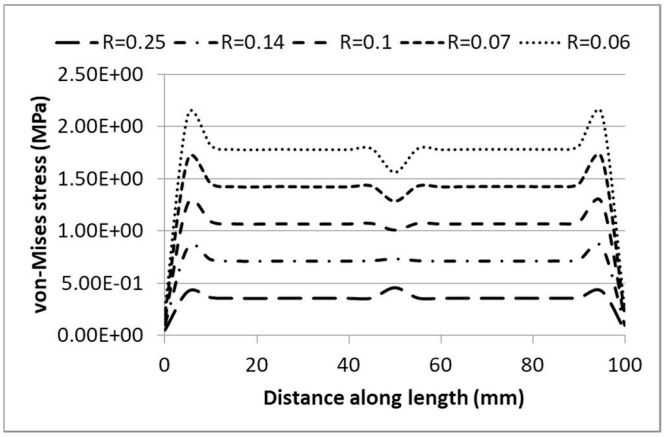

(b)

Fig. 12. Von-Mises stress (vol. % = 20) (a) Untreated (b) Treated SFRPC samples.

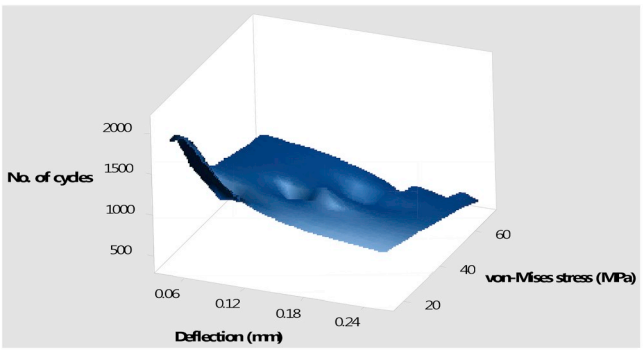

(a)

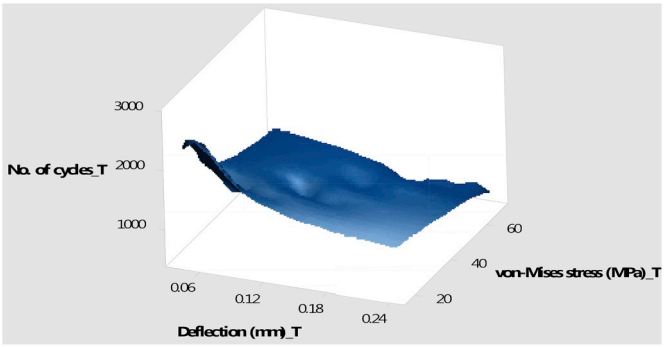

(b)

Fig. 14. The life-stress-strain plots for the (a) untreated and (b) treated SERPC samples.

the similar trends the bubble plots for untreated SFRPC samples are given in Fig. 7 (a) and (b). The bubble plot clearly indicates the linear positive trend for R and no. of cycles, not much variation in bubble size highlights the consistency of data and a very strong relation between R and no. of cycles and strong relation between proportion (%) and no. of cycles for all the tested values. The treated SFRPC samples have shown a competitive CFS to the carbon fiber reinforced epoxy composites [24].

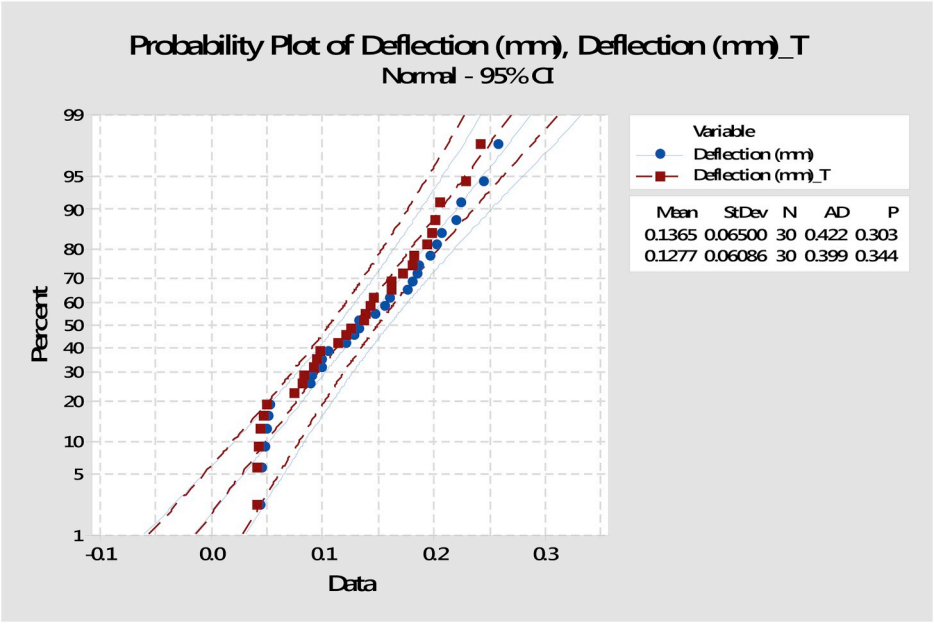

Fig. 13. The probability plots for deflection of the untreated and treated SERPC samples.

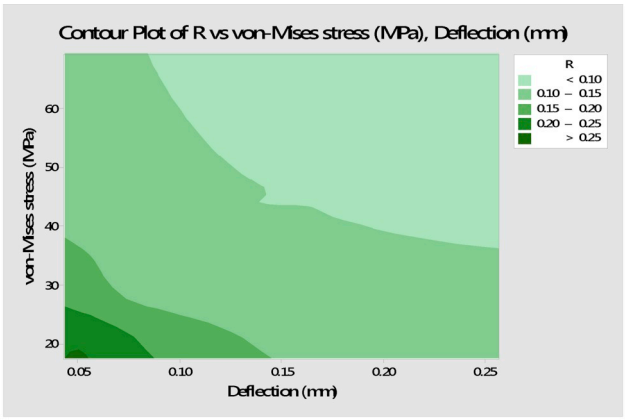

(a)

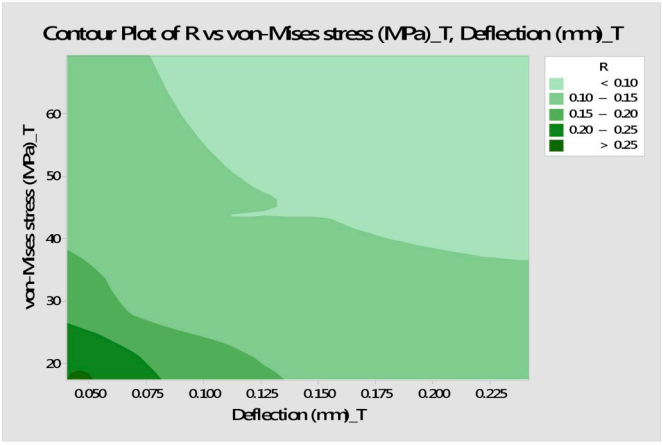

(b)

Fig. 15. The contour plots of R-stress-deflection for the (a) untreated and (b) treated SERPC samples.

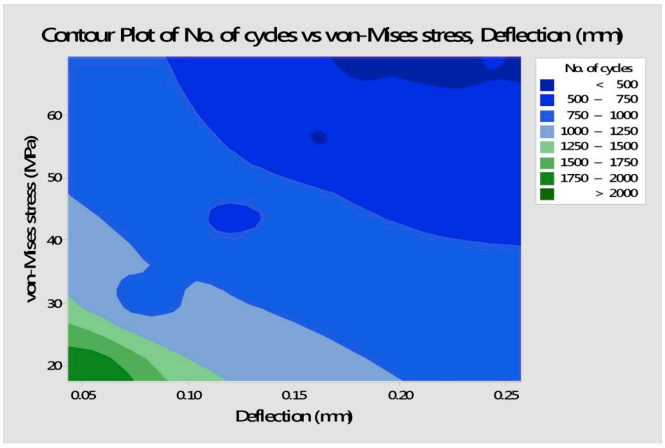

(a)

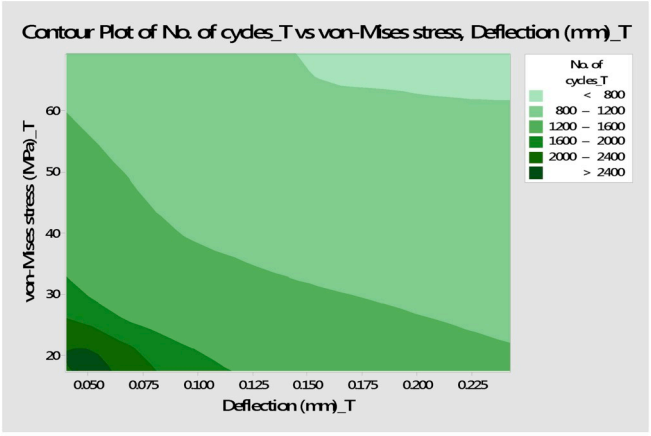

(b)

Fig. 16. The contour plots of life-stress-deflection for the (a) untreated and (b) treated SERPC samples.

An earlier reported study by the author shows that treated SFRPC composites has the higher life for the same value of R than the carbon fiber reinforced epoxy composites [24]. Such encouraging results open a new horizon for the utilization of the low-cost natural fiber composites for the fatigue prone structures.

3.2. Finite element analysis

Fig. 8 (a) shows the variation of predicted Young's modulus for the developed composites. It was observed that both the untreated as well as treated composites exhibited an invariable increase in Young's modulus with bagasse particle proportions. The treated particles displayed the higher value of Young's modulus for all proportions. This is attributed to the enhanced stiffness imparted to the epoxy matrix due to the glass powder modification of BPs. Similar behaviour has been observed in the experimental results of Wang et al. [13] and Ku et al. [30]. The FE results are consistent with the present experimental results in the way that the enhanced stiffness of composites with treated particles attributes to the enhanced fatigue life of composites. Possibly the BPs showed the lesser reinforcing capability without the treatment. Fig. 8(b) shows the variation of the predicted Poisson's ratio for the untreated and treated SFRPC composites. A slight reduction with concentration was observed with both untreated as well as treated particles. The treated particles displayed lower Poisson's ratio in the comparison with the untreated once. This is attributed to the smaller Poisson's ratio of glass particles as shown in Table 1.

Fig. 9 shows the direct and Von-Mises stress contours in the representative volume element (RVE) subjected to an applied bending stress of 100 MPa in Z-direction. The results were obtained for the bagasse fiber concentration of 25%. The equatorial location of epoxy at the particle-epoxy interface was observed to be under small stress concentration in the case of both treated as well as untreated BPs as shown in Fig. 9 (a) and (c). On the other hand, the concentration of stress was observed at the polar location of the untreated bagasse particle as shown in Fig. 9 (b). The maximum stress concentration zone shifted to the center of the treated bagasse particle as shown in Fig. 9 (e).

In case of treated particles, the glass powder layer was observed to be under a very high stress at its equatorial position. Such high-stress concentration might have caused the fracture of the glass layer first under fatigue loading due to its brittle nature. In order to simulate the effect of fracture of the glass layer, it was modeled as a low-stiffness material. Such an assumption seems to be valid as the glass layer loses its stiffness after the fracture has taken place. Fig. 9 (g-i) shows the stress distributions under this condition. It can be observed that as the glass layer fails, the Von-Mises stress increases in the epoxy matrix. It appears that the fracture of glass layer has resulted in the creation of void and subsequent enhancement in the Von-Mises stress leading to localized shear yielding. This shear yielding might have led to the enhanced fatigue strength of the composites with treated particles [73].

Fig. 10 (a) and (b) show the sample simulation results for the distribution of Von-Mises stresses and deflection for untreated SFRPCs at

R = 0.07, Proportion (%) = 20%, N = 500 respectively. Fig. 11 shows the sample simulation outputs giving the mid line deflection for untreated and treated samples. Fig. 12 (a) and (b) give the associated values of Von-Mises stresses. The complete results are summarized in Table 2.

Fig. 13 shows the probability plot for the deflection in treated/untreated SFRPCs. The probability plot indicates that data follow the normal distribution and a good fit. The mean values of deflection for untreated and treated SFRPCs were 0.1365 and 0.1277 mm respectively. On an average, the treated SFRPCs showed 6.44% lesser deflection than the untreated SFRPCs displaying. The standard deviation of treated SFRPCs (0.06086) was also observed to be lower than the untreated SFRPCs (0.06500) exhibiting lower variability in data and higher uniformity of treatment.

The surface plots (Fig. 14 (a) and (b)) represent the stress-deformation-life relation for untreated and treated SFRPC samples (method 4). The longer life, lower deflection at higher stresses in the case of treated SFRPC samples is clearly visible from surface plots.

Fig. 15 (a) and (b) shows the R versus Von-Mises stress and deflection contour plots for untreated as well as treated SFRPC samples. It can be observed that in both cases, the Von-Mises stress, as well as the deflection, increased significantly with the reduction in R.

Fig. 16 (a) and (b) shows the number of cycles to failure versus Von-Mises stress and deflection contour plots for untreated as well as treated SFRPC samples. It can be observed that in both cases, the SFRPCs exhibited higher deflection and Von-Mises stress at a lower number of cycles. At a lower number of cycles, the deflection and Von-Mises stress were observed to be significantly higher in both the cases.

The fractured SFRPCs were examined using the SEM micrographs (Fig. 17 (a) and (b)). The matrix debonding at the interface was clearly visible for the untreated SFRPC samples signifying inadequate bonding at the matrix-fiber. On the other hand, the SEM micrographs for treated SFRPCs exhibited the retarded tendency of matrix debonding and fiber pullout. This is due to the presence of the glass powder on the surface of SFs. The glass powder has enhanced the interfacial friction between matrix and SFs leading to mechanical interlocking. The mechanical interlocking is the main strengthening mechanism active at the interface and is the reason behind the enhanced life of treated samples. In addition to this, the glass powder treated SFs have a higher contact area, leading to better contact at between the matrix and SFs. On the other hand, the micrographs of untreated SFRPC samples displayed brittle fracture manifested by the rapid propagation of cracks in multiple directions. The treated samples displayed plastic deformation prior to failure. This is manifested in the enhanced fatigue life of the treated samples at all proportions in comparison to the untreated ones. The

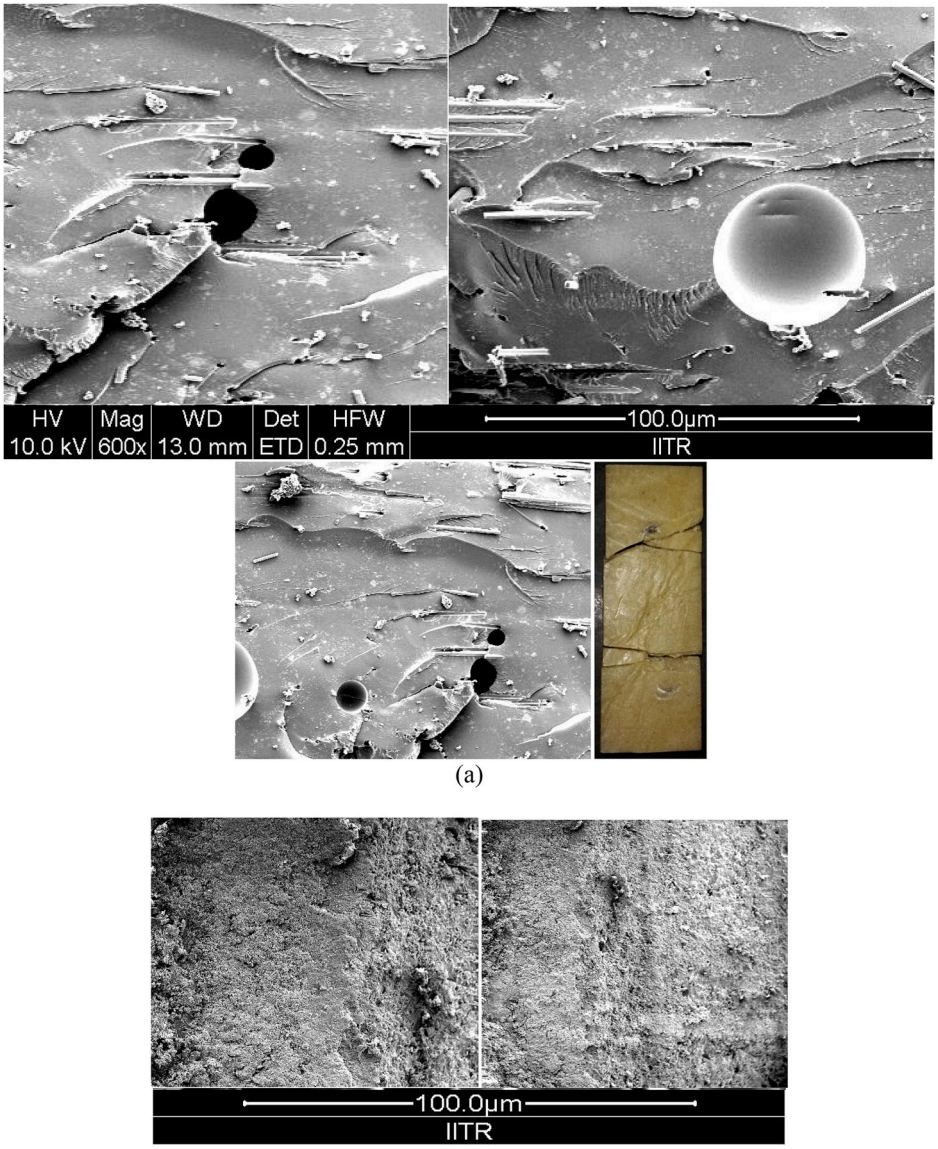

Fig. 17. SEM Micrographs of fractured surfaces and fractured (a) Untreated (b) Treated SFRPC samples.

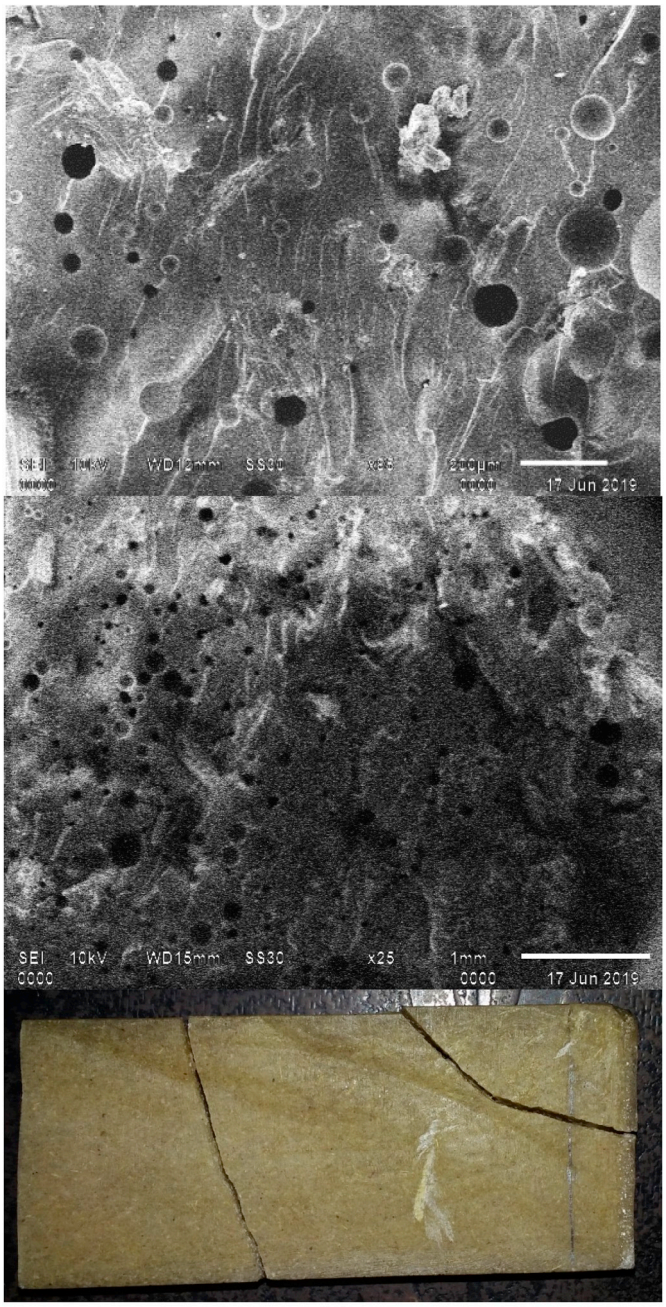

(b)

Fig. 17. (*continued*).

plastic deformation is also observed in the micromechanical FE model of the treated SFRPC (Fig. 9). The glass powder layer might have fractured due to high-stress concentration. Its fracture gives rise to increased Von-Mises stress in the matrix leading to its plastic deformation due to localized yielding [73].

The surface modification of SFs using the glass powder has significantly enhanced the fiber-matrix interface by altering the surface morphology of the SFs. Moreover, as exhibited by the FE model, the increase in Von-Mises stress due to fracture of the glass powder layer has induced localized shear yielding of the matrix leading to enhanced fatigue life.

The surface modification of sugar cane fibers using the glass powder has shown a significant effect on the fiber–matrix interaction and the surface morphology of the sugar cane fibers. Thus, the treatment of sugar cane fibers before incorporating them in the epoxy matrix proved to have a significant effect in enhancing the CFS of SFRPCs by interface strengthening. A similar effect was observed due to the treatment of carbon fibers with the glass powder [24]. The continuum assumptions in the numerical model might have shortcomings as the nano-flaws visible in SEM images of the treated/untreated SFRPCs. A model that considers the nano-flaws and the discrete nature the SFRPCs and correlates the nano and macro level fracture could be considered as the work for the future. The fatigue-crack-growth-regions with distinct striations occasionally were visible in fractured SFRPC samples due to the non-uniform crack extension and larger striation spacing. The nano plastic zone at the crack tip was formed and due to the repeated and varying load divided into many crack branches which were propagated in the encouraging directions. The favourable direction of crack propagation during the fracture of SFRPCS was based on the presence of flows nearby the crack propagation route and availability of the least energy required to break

the single bond at the crack tip. A numerical model customized for SFRPCs which can handle non-homogeneity, the multiple fractures, pre-existing cracks, voids, and defects can be considered as future work. Additionally, assuming SFRPCs a linear elastic material is a simplification and SFRPCs are sensitive to the loading rate, temperature and might have the nonlinear stress-strain behavior. The FE model employed in the present work paper could be enhanced through the incorporation of three-dimensional images from sophisticated technique such as tomography. Although, studies have been made to generate artificial microstructure of composites and study defects such as clustering and void formation; still, sophisticated techniques such as holotomography and computed tomography are imperative for developing complete understanding of the Nano and micro flaws present in the composites. The images obtained from such techniques can be directly transferred to finite element packages and further analysis can be done. However, such sophisticated techniques are coupled with infrastructural as well as computational difficulties The structure-property relationship could be better explained if the TEM, DTA, FT-IR, thermal gravimetric, EDS, XRD results were also available, however, this will be considered as the future work.

4. Conclusions

The treatment of sugar cane fibers by glass powder is an inexpensive and effective method for improving the CFS of SFRPCs. The treated SFRPC samples have a higher CFS, life, and lower deflection than the untreated SFRPCs. The life of the SFRPC samples (treated/untreated) exponential vary with load. The 25% volume proportion of sugar cane fiber has resulted in the higher life for treated/untreated SFRPC sample. The treated SFRPC samples were having higher average fatigue life than the CFRPC samples. The ANOVA results have confirmed CFS dependability on R, treatment effect and R was prominent among two. The higher Von-Mises stress of the glass powder layer of sugar cane fiber has induced localized shear yielding of the matrix leading to enhanced fatigue life. The mechanical anchoring and roughness due to the treatment resulted in interface strengthening and enhanced fiber strength which in turn resulted in the longer life of treated SFRPC samples than the untreated LG samples. The developed FE model based on the representative volume (numerical homogenization technique) approach has predicted elastic properties of SFRPC and macro-mechanical FE model (transient analysis) has predicted stress and deformation for different values of R, proportion, and no. of cycles. The reported FE models were in line with the experiments and complemented the experimental results well. However, a requirement of highly specialized numerical algorithm to model the effect of treatment method and flaws was noticed.

Acknowledgments

Present work is by Invertis University, Bareilly, (U.P.), India. The financial support by IAAM, Sweden is highly acknowledged.

References

[1] Sugarcane production in 2016, crops/regions/world list/production quantity (pick lists)". UN food and agriculture organization, corporate statistical database (FAOSTAT). 2017.
[2] Ogden JM, Hochgreb S, Hylton M. Steam economy and cogeneration in cane sugar factories. Int Sugar J 1990;92(1099):131–43. 1.
[3] Ribeiro Filho SL, Oliveira PR, Panzera TH, Scarpa F. Impact of hybrid composites based on rubber tyres particles and sugarcane bagasse fibres. Compos B Eng 2019;15(159):157–64. https://doi.org/10.1016/j.compositesb.2018.09.054.
[4] Ravindranath NH, Balachandra P, Dasappa S, Rao KU. Bioenergy technologies for carbon abatement. Biomass Bioenergy 2006;30(10):826–37. 1, https://doi.org/10.1016/j.biombioe.2006.02.003.
[5] Wambua P, Ivens J, Verpoest I. Natural fibres: can they replace glass in fibre reinforced plastics? Compos Sci Technol 2003;63(9):1259–64. Jul 1, https://doi.org/10.1016/S0266-3538(03)00096-4.
[6] Pickering KL, Efendy MA, Le TM. A review of recent developments in natural fibre composites and their mechanical performance. Compos Part A Appl S 2016;83:98–112. 1, https://doi.org/10.1016/j.compositesa.2015.08.038.
[7] Tiwari S, Bijwe J, Panier S. Gamma radiation treatment of carbon fabric to improve the fiber–matrix adhesion and tribo-performance of composites. Wear 2011;271(9–10):2184–92. 29, https://doi.org/10.1016/j.wear.2010.11.032.
[8] Adekunle KF. Surface treatments of natural fibres—a review: Part 1. Open J Polym Chem 2015;5(03):41. https://doi.org/10.4236/ojpchem.2015.53005. 6.
[9] Deepa B, Abraham E, Cherian BM, Bismarck A, Blaker JJ, Pothan LA, Leao AL, De Souza SF, Kottaisamy M. Structure, morphology and thermal characteristics of banana nano fibers obtained by steam explosion. Bioresour Technol 2011;102(2):1988–97. 1, https://doi.org/10.1016/j.biortech.2010.09.030.
[10] Ragoubi M, George B, Molina S, Bienaimé D, Merlin A, Hiver JM, Dahoun A. Effect of corona discharge treatment on mechanical and thermal properties of composites based on miscanthus fibres and polylactic acid or polypropylene matrix. Compos Part A Appl S 2012;43(4):675–85. 1, https://doi.org/10.1016/j.compositesa.2011.12.025.
[11] Huda MS, Drzal LT, Mohanty AK, Misra M. Effect of fiber surface-treatments on the properties of laminated biocomposites from poly (lactic acid)(PLA) and kenaf fibers. Compos Sci Technol 2008;68(2):424–32. https://doi.org/10.1016/j.compscitech.2007.06.022.
[12] Sawpan MA, Pickering KL, Fernyhough A. Flexural properties of hemp fibre reinforced polylactide and unsaturated polyester composites. Compos Part A Appl S 2012;43(3):519–26. 1, https://doi.org/10.1016/j.compositesa.2011.11.021.
[13] Wang H, Han W, Tian H, Wang Y. The preparation and properties of glass powder reinforced epoxy resin. Mater Lett 2005;59(1):94–9. 1, https://doi.org/10.1016/j.matlet.2004.09.024.
[14] Onésippe C, Passe-Coutrin N, Toro F, Delvasto S, Bilba K, Arsène MA. Sugar cane bagasse fibres reinforced cement composites: thermal considerations. Compos Part A Appl S 2010;41(4):549–56. 1, https://doi.org/10.1016/j.compositesa.2010.01.002.
[15] Moubarik A, Grimi N, Boussetta N. Structural and thermal characterization of Moroccan sugar cane bagasse cellulose fibers and their applications as a reinforcing agent in low density polyethylene. Compos B Eng 2013;52:233–8. 1, https://doi.org/10.1016/j.compositesb.2013.04.040.
[16] Vilay V, Mariatti M, Taib RM, Todo M. Effect of fiber surface treatment and fiber loading on the properties of bagasse fiber–reinforced unsaturated polyester composites. Compos Sci Technol 2008;68(3–4):631–8. 1, https://doi.org/10.1016/j.compscitech.2007.10.005.
[17] Nagakalyan S, Anoopisan, Vijaykiran B. Interfacial behavior of composites of polymer and sugarcane fiber. Int J Innovative Res Adv Eng 2015;7(2). 2349-2163.
[18] Luz SM, Goncalves AR, Del'Arco Jr AP. Mechanical behavior and microstructural analysis of sugarcane bagasse fibers reinforced polypropylene composites. Compos Part A Appl S and manufacturing 2007;38(6):1455–61. 1, https://doi.org/10.1016/j.compositesa.2007.01.014.
[19] Miléo PC, Mulinari DR, Baptista CA, Rocha GJ, Gonçalves AR. Mechanical behaviour of polyurethane from castor oil reinforced sugarcane straw cellulose composites. Procedia Eng 2011;10:2068–73. 1, https://doi.org/10.1016/j.proeng.2011.04.342.
[20] Sahari J, Sapuan SM, Zainudin ES, Maleque MA. Mechanical and thermal properties of environmentally friendly composites derived from sugar palm tree. Mater Des 2013;49:285–9. 1, https://doi.org/10.1016/j.matdes.2013.01.048.
[21] Agunsoye JO, Aigbodion VS. Bagasse filled recycled polyethylene bio-composites: morphological and mechanical properties study. Results Phys 2013;3:187–94. 1, https://doi.org/10.1016/j.rinp.2013.09.003.
[22] Paluvai NR, Mohanty S, Nayak SK. Synthesis and modifications of epoxy resins and their composites: a review. Polym Plast Technol 2014;53(16):1723–58. 20, https://doi.org/10.1080/03602559.2014.919658.
[23] Roşu D, Caşcaval CN, Mustată F, Ciobanu C. Cure kinetics of epoxy resins studied by non-isothermal DSC data. Thermochim Acta 2002;383(1–2):119–27. 7, https://doi.org/10.1016/S0040-6031(01)00672-4.
[24] Vedrtnam A. Novel method for improving fatigue behavior of carbon fiber reinforced epoxy composite. Compos B Eng 2019;157:305–21. 15, https://doi.org/10.1016/j.compositesb.2018.08.062.
[25] Sood M, Dwivedi G. Effect of fiber treatment on flexural properties of natural fiber reinforced composites: a review. Egypt J Petrol 2017. 20, https://doi.org/10.1016/j.ejpe.2017.11.005.
[26] Sharma M, Gao S, Mäder E, Sharma H, Wei LY, Bijwe J. Carbon fiber surfaces and composite interphases. Compos Sci Technol 2014;102:35–50. 6, https://doi.org/10.1016/j.compscitech.2014.07.005.
[27] Brocks T, Cioffi MO, Voorwald HJ. Effect of fiber surface on flexural strength in carbon fabric reinforced epoxy composites. Appl Surf Sci 2013;274:210–6. 1, https://doi.org/10.1016/j.apsusc.2013.03.018.
[28] Saba N, Tahir P, Jawaid M. A review on potentiality of nano filler/natural fiber filled polymer hybrid composites. Polym 2014;6(8):2247–73. https://doi.org/10.3390/polym6082247.
[29] Saba N, Tahir P, Jawaid M. A review on potentiality of nano filler/natural fiber filled polymer hybrid composites. Polymers 2014;6(8):2247–73. https://doi.org/10.3390/polym6082247.
[30] Le Moigne N, Sonnier R, El Hage R, Rouif S. Radiation-induced modifications in natural fibres and their biocomposites: opportunities for controlled physico-chemical modification pathways? Ind Crops Prod 2017;109:199–213. 15, https://doi.org/10.1016/j.indcrop.2017.08.027.
[31] Ku H, Wong P, Huang J, Fung H, Trada M. Tensile tests of glass powder reinforced epoxy composites: pilot study. Adv Mater Res 2011;214:1–5. Trans Tech Publications, https://doi.org/10.4028/www.scientific.net/AMR.214.1.
[32] Voss H, Karger-Kocsis J. Fatigue crack propagation in glass-fibre and glass-sphere filled PBT composites. Int J Fatigue 1988;10(1):3–11. 1, https://doi.org/10.1016/0142-1123(88)90015-1.

[33] Kawaguchi T, Pearson RA. The moisture effect on the fatigue crack growth of glass particle and fiber reinforced epoxies with strong and weak bonding conditions: Part 2. A microscopic study on toughening mechanism. Compos Sci Technol 2004; 64(13–14):1991–2007. 1, https://doi.org/10.1016/j.compscitech.2004.02.017.
[34] Węcławski BT, Fan M, Hui D. Compressive behaviour of natural fibre composite. Compos B Eng 2014;67:183–91. 1, https://doi.org/10.1016/j.compositesb.2014.07.014.
[35] Chegdani F, Wang Z, El Mansori M, Bukkapatnam ST. Multiscale tribo-mechanical analysis of natural fiber composites for manufacturing applications. Tribol Int 2018;122:143–50. 1, https://doi.org/10.1016/j.triboint.2018.02.030.
[36] Sailesh A, Arunkumar R, Saravanan S. Mechanical properties and wear properties of kenaf–aloe vera–jute fiber reinforced natural fiber composites. Mater Today-Proc 2018;5(2):7184–90. 31, https://doi.org/10.1016/j.matpr.2017.11.384.
[37] Vedrtnam A, Pawar SJ. Experimental and simulation studies on fatigue behavior of laminated glass having polyvinyl butyral and ethyl vinyl acetate interlayers. Fatigue Fract Eng M 2018;41(6):1437–46. https://doi.org/10.1111/ffe.12788.
[38] Vedrtnam A. Novel method for improving fatigue behaviour of laminated glass. Fatigue Fract Eng M 2019;42(2):504–17. https://doi.org/10.1111/ffe.12926.
[39] Vedrtnam A. Novel treatment methods for improving fatigue behavior of laminated glass. Compos B Eng 2019;167:180–98. 15, https://doi.org/10.1016/j.compositesb.2018.12.037.
[40] Bisen HB, Hirwani CK, Satankar RK, Panda SK, Mehar K, Patel B. Numerical study of frequency and deflection responses of natural fiber (Luffa) reinforced polymer composite and experimental validation. J Nat Fibers 2018;16:1–5. https://doi.org/10.1080/15440478.2018.1503129.
[41] Hirwani CK, Panda SK, Patle BK. Theoretical and experimental validation of nonlinear deflection and stress responses of an internally debonded layer structure using different higher-order theories. Acta Mech 2018;229(8):3453–73. 1, https://doi.org/10.1007/s00707-018-2173-8.
[42] Hirwani CK, Panda SK. Nonlinear finite element solutions of thermoelastic deflection and stress responses of internally damaged curved panel structure. Appl Math Model 2019;65:303–17. 1, https://doi.org/10.1016/j.apm.2018.08.014.
[43] Hirwani CK, Panda SK. Numerical and experimental validation of nonlinear deflection and stress responses of pre-damaged glass-fibre reinforced composite structure. Ocean Eng 2018;159:237–52. 1, https://doi.org/10.1016/j.oceaneng.2018.04.035.
[44] Hirwani CK, Panda SK, Mahapatra TR. Thermomechanical deflection and stress responses of delaminated shallow shell structure using higher-order theories. Compos Struct 2018;184:135–45. 15, https://doi.org/10.1016/j.compstruct.2017.09.071.
[45] Tucker III CL, Liang E. Stiffness predictions for unidirectional short-fiber composites: review and evaluation. Compos Sci Technol 1999;59(5):655–71. 1, https://doi.org/10.1016/S0266-3538(98)00120-1.
[46] Zhang D, Milanovic NR, Zhang Y, Su F, Miao M. Effects of humidity conditions at fabrication on the interfacial shear strength of flax/unsaturated polyester composites. Compos B Eng 2014;60:186–92. 1, https://doi.org/10.1016/j.compositesb.2013.12.031.
[47] Sliseris J, Yan L, Kasal B. Numerical modelling of flax short fibre reinforced and flax fibre fabric reinforced polymer composites. Compos B Eng 2016;89:143–54. 15, https://doi.org/10.1016/j.compositesb.2015.11.038.
[48] Modniks J, Andersons J. Modeling elastic properties of short flax fiber-reinforced composites by orientation averaging. Comput Mater Sci 2010;50(2):595–9. 1, https://doi.org/10.1016/j.commatsci.2010.09.022.
[49] Modniks J, Andersons J. Modeling the non-linear deformation of a short-flax-fiber-reinforced polymer composite by orientation averaging. Compos B Eng 2013;54: 188–93. 1, https://doi.org/10.1016/j.compositesb.2013.04.058.
[50] Brighenti R, Carpinteri A, Scorza D. Mechanics of interface debonding in fibre-reinforced materials. J Compos Mater 2016;50(19):2699–718. https://doi.org/10.1177/0021998315612537.
[51] Xu Z, Li J, Wu X, Huang Y, Chen L, Zhang G. Effect of kidney-type and circular cross sections on carbon fiber surface and composite interface. Compos Part A Appl S 2008;39(2):301–7. 1, https://doi.org/10.1016/j.compositesa.2007.10.015.
[52] Barbieri G, Biolzi L, Bocciarelli M, Cattaneo S. Size and shape effect in the pull-out of FRP reinforcement from concrete. Compos Struct 2016 20;143:395–417. https://doi.org/10.1016/j.compstruct.2016.01.097.
[53] Jäger J, Sause MG, Burkert F, Moosburger-Will J, Greisel M, Horn S. Influence of plastic deformation on single-fiber push-out tests of carbon fiber reinforced epoxy resin. Compos Part A Applied S 2015;71:157–67. 1, https://doi.org/10.1016/j.compositesa.2015.01.011.
[54] Wang H, Xiao Y, Qin QH. 2D hierarchical heat transfer computational model of natural fiber bundle reinforced composite. Sci Iran. Trans B. 2016 1;23(1):268.
[55] Ilczyszyn F, Cherouat A, Montay G. Effect of hemp fibre morphology on the mechanical properties of vegetal fibre composite material. Adv Mater Res 2014; 875:485–9. Trans Tech Publications, https://doi.org/10.4028/www.scientific.net/AMR.875-877.485.
[56] Nilsson T, Gustafsson PJ. Influence of dislocations and plasticity on the tensile behaviour of flax and hemp fibres. Compos Part A-Appl S 2007;38(7):1722–8. 1, https://doi.org/10.1016/j.compositesa.2007.01.018.
[57] Xiong X, Shen SZ, Hua L, Liu JZ, Li X, Wan X, Miao M. Finite element models of natural fibers and their composites: a review. J Reinf Plast Compos 2018;37(9): 617–35. https://doi.org/10.1177/0731684418755552.
[58] Gassan J. A study of fibre and interface parameters affecting the fatigue behaviour of natural fibre composites. Compos Part A appl S 2002;33(3):369–74. 1, https://doi.org/10.1016/S1359-835X(01)00116-6.
[59] Spearing SM, Beaumont PW. Fatigue damage mechanics of composite materials. I: experimental measurement of damage and post-fatigue properties. Compos Sci Technol 1992;44(2):159–68. 1, https://doi.org/10.1016/0266-3538(92)90109-G.
[60] Spearing SM, Beaumont PW, Ashby MF. Fatigue damage mechanics of composite materials. II: a damage growth model. Compos Sci Technol 1992;44(2):169–77. 1, https://doi.org/10.1016/0266-3538(92)90110-O.
[61] Putić S, Uskoković PS, Aleksić R. Analysis of fatigue and crack growth in carbon-fiber epoxy matrix composite laminates. Strength Mater+ 2003;35(5):500–7. 1, https://doi.org/10.1023/B:STOM.0000004538.77270.1e.
[62] Gunwant D, Sah PL, Zaidi MG. Morphology and micromechanics of liquid rubber toughened epoxies. E-Polymers 2018;18(6):511–27. 25, https://doi.org/10.1515/epoly-2018-0141.
[63] Shoukry SN, Prucz JC, Shankaranarayana PG, William GW. Microstructure modeling of particulate reinforced metal matrix composites. Mech Adv Mater Struct 2007;14(6):499–510. 21, https://doi.org/10.1080/15376490701410497.
[64] Vedrtnam A. Experimental and simulation studies on delamination strength of laminated glass composites having polyvinyl butyral and ethyl vinyl acetate interlayers of different critical thicknesses. Defence Technol 2018;14(4):313–7. 1, https://doi.org/10.1016/j.dt.2018.02.002.
[65] Vedrtnam A, Pawar SJ. Experimental and simulation studies on fracture and adhesion test of laminated glass. Eng Fract Mech 2018;190:461–70. 1, https://doi.org/10.1016/j.engfracmech.2017.12.044.
[66] Balaji A, Karthikeyan B, Raj CS. Bagasse fiber–the future biocomposite material: a review. Int J Cemtech Res 2014;7(1):223–33.
[67] Vedrtnam A, Pawar SJ. Experimental and simulation studies on flexural strength of laminated glass using ring-on-ring and three-point bending test. Proc Inst Mech Eng, Part C-J Mech Eng Sci 2018;232(21):3930–41. https://doi.org/10.1177/0954406217744815.
[68] Vedrtnam A. Comparative evaluation of novel thermo-chemical treatment methods for improved impact performance of laminated glass. Proc Inst Mech Eng, Part C-J Mech Eng Sci 2019;233(4):1334–44. https://doi.org/10.1177/0954406218771995.
[69] Constantinescu DM, Apostol DA, Picu CR, Krawczyk K, Sieberer M. Mechanical properties of epoxy nanocomposites reinforced with functionalized silica nanoparticles. Procedia Struct Int 2017;5:647–52. 1, https://doi.org/10.1016/j.prostr.2017.07.034.
[70] Boonyapookana A, Nagata K, Mutoh Y. Fatigue crack growth behavior of silica particulate reinforced epoxy resin composite. Compos Sci Technol 2011;71(8): 1124–31. 31, https://doi.org/10.1016/j.compscitech.2011.02.015.
[71] Kawaguchi T, Pearson RA. The moisture effect on the fatigue crack growth of glass particle and fiber reinforced epoxies with strong and weak bonding conditions: Part 1. Macroscopic fatigue crack propagation behavior. Compos Sci Technol 2004; 64(13–14):1981–9. 1, https://doi.org/10.1016/j.compscitech.2004.02.016.
[72] Ferreira JA, Borrego LP, Costa JD, Capela C. Fatigue behaviour of nanoclay reinforced epoxy resin composites. Compos B Eng 2013;52:286–91. 1, https://doi.org/10.1016/j.compositesb.2013.04.003.
[73] Borrego LP, Costa JD, Ferreira JA, Silva H. Fatigue behaviour of glass fibre reinforced epoxy composites enhanced with nanoparticles. Compos B Eng 2014;62: 65–72. 1, https://doi.org/10.1016/j.compositesb.2014.02.016.